Synthesis and Characterization of Mn Doped CuO Nanostructures

MS Thesis

By

Muhammad Sajid
Reg: No: 297-FBAS/MSPHY/F14

Supervisor
Dr. Javed Iqbal Saggu
Department of Physics

Faculty of Basic and Applied Sciences
International Islamic University, Islamabad

(2016)

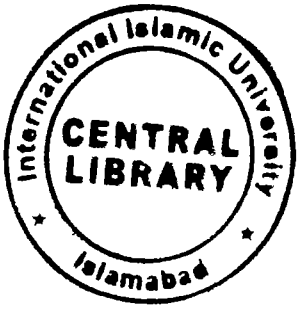

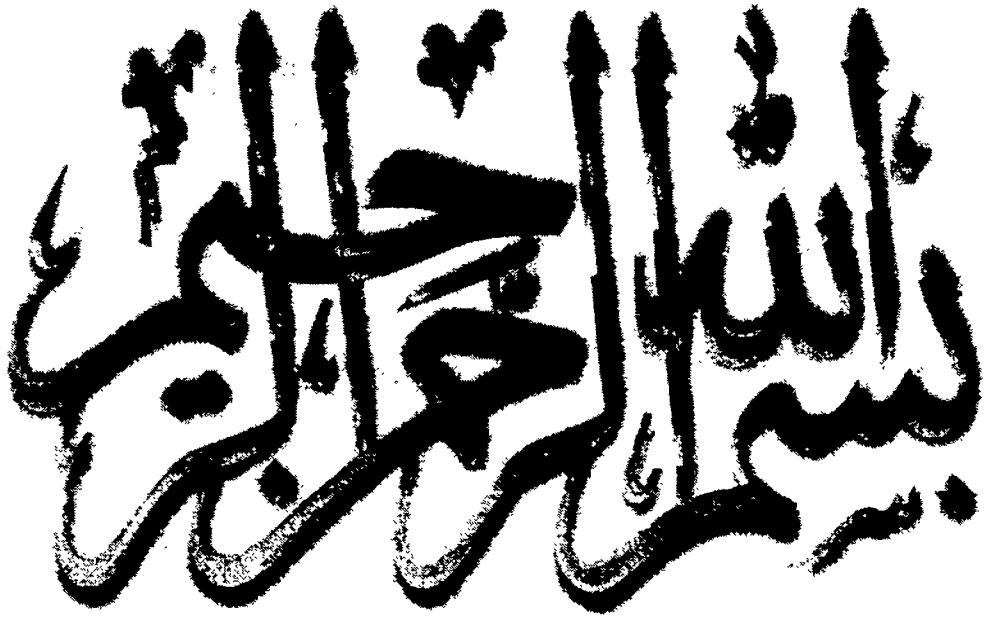

Certificate

This is to certify that Mr. **Muhammad Sajid** has carried out the work in this thesis entitled **"Synthesis and Characterization of Mn Doped CuO Nanostructures"** under my supervision in the laboratory of Nanoscience and Technology (LNT) and is accepted in its present form by the Department of Physics, International Islamic University Islamabad as satisfying the thesis requirement for the degree of MS Physics.

Dr. Javed Iqbal Saggu

Supervisor

Department of Physics,

Quaid-i-Azam University, Islamabad

Synthesis and Characterization of Mn Doped CuO Nanostructures

By

Muhammad Sajid
Reg: No: 297-FBAS/MSPHY/F14

A thesis submitted to
Department of Physics, FBAS, IIUI

For the award of the degree of
MS Physics

Signature: 

(Chairman, Department of Physics, FBAS, IIUI)

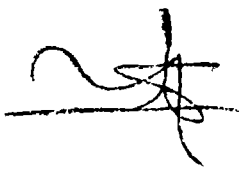

Signature: _____

(Dean, FBAS, IIUI)

FINAL APPROVAL

It is certified that the work presented in this thesis entitled **"Synthesis and Characterization of Mn Doped CuO Nanostructures"** by **Mr. Muhammad Sajid** bearing **Registration No. 297-FBAS/MSPHY/F14** is of sufficient standard in scope and quality for the award of degree of MS Physics from International Islamic University, Islamabad.

COMMITTEE

External Examiner

Dr. Ishaq Ahmad
National Centre for Physics
Islamabad

Internal Examiner

Dr. Waqar Adil Syed
Chairman Department of Physics,
FBAS, IIUI.

Supervisor

Dr. Javed Iqbal Saggu
Department of Physics,
FBAS, IIUI.

Declaration

I hereby declare that this thesis work, neither as a whole nor a part of it has been copied out from any source. Further, work presented in this dissertation has not been submitted in support of any application for any other degree or qualification to any other university or institute and is considerable under the plagiarism rules of Higher Education Commission (HEC), Pakistan.

Signature: M. Sajid

Muhammad Sajid

Registration No: 297-FBAS/MSPHY/F14

Dedicated

To

My Beloved Parents,

My Brother

Mr. Muhammad Saleem,

Loving Friends and Teachers

ACKNOWLEDGEMENTS

It gives me great pleasure and satisfaction to acknowledge the endowment of the creator of the universe, **Allah Almighty**, the most gracious, compassionate and beneficent to His creature, which enabled me to complete my research work successfully. I offer my humblest and sincere words of thanks to the **Holy Prophet Muhammad (P.B.U.H)** who is forever a source of guidance and knowledge for humanity.

This work would have not been possible without the invaluable contributions of many individuals. First and foremost, I wish to thank my reverend supervisor **Dr. Javed Iqbal Saggu** for all of his support, advice, and guidance during the whole period of my research work.

I need to acknowledge some individuals on the personal side of my life, my sincerest gratitude loving parents, my Brother Mr. Muhammad Saleem and Uncles Mr. Muhammad Tufail and Mr. Fazal Hussain. I could not wish for a more supportive, loving family and for them I am deeply thankful and blessed.

I am very much grateful to all my seniors Ms. Aqsa Arshad, Dr. Tariq Jan, Mr. Umar Farooq and Mr. Umair Ali Sabir, my research fellows Mr. Abid Alam, Mr. Salahuddin and Mr. Basit Ali Shah for their help and support during my research work in the Laboratory of Nanoscience and Technology (LNT).

Muhammad Sajid

Abstract

Nanostructures transition metal oxides (TMOs), a particular class of nanomaterials that are considered to be foundation for the development of various novel functional and smart materials. Among these, copper oxide (CuO) nanostructures have unique size and dimensionally dependent physical and chemical properties which make them attractive not only for the fundamental scientific research, but also for various practical applications in the field of material science and engineering. In this thesis, an effort is made to study the undoped and Mn doped CuO nanostructures that have been synthesized by a simple chemical coprecipitation method. The prepared samples have been characterized using different characterization techniques i.e. X-ray diffraction (XRD), Scanning electron microscopy (SEM), Energy dispersive x-ray spectroscopy (EDX), Fourier transform infrared spectroscopy (FTIR), UV-Visible spectroscopy (UV- Vis) and Dielectric behavior. The structural results reveal the formation of pure single phase monoclinic nanostructures of CuO for all the prepared samples. Scherer's formula has been used to calculate the crystalline size which exhibits an increasing trend from 19.54 nm to 24.03 nm as a function of Mn doping into host matrix. SEM results have shows the nanorods like morphology which changes to nano particles as a function of Mn doping. FTIR results illustrate the presence of various functional groups and vibrational modes in prepared samples. This further conform monoclinic structure. UV-Vis analysis suggests the band gap of the synthesized nanostructure of CuO decreases as the amount of Mn increases. While dielectric constant of the prepared samples increases with Mn doping in the host matrix.

Table of Contents

List of Figures

List of Tables

CHAPTER NO: 01

INTRODUCTION

1.1 Nanotechnology

Nanotechnology is the science of materials conducting at nanoscale. Where as one nanometer equal to one billionth of a meter i.e. 10^{-9} of a meter, also one nanometer is equivalent to 5 silicon or 10 hydrogen atoms align side by side The thought of Nanoscience is often refer to a famous idea entitled "**There's Plenty of Room at The Bottom**" by a one the famous physicist Richard Feynman, in 1959 at an American Physical Society meeting.

1.2 Classification of Nanostructured Materials (NSMs)

Nanotechnology is the study of matter at atomic and molecular scale or in nano meter range. It shows tremendous applications in various fields such as physics, biology, material science and chemistry. Therefore many and unique nano scales materials are developed in the past two decades, and it has become necessary to classify these nano materials for batter understanding. Gleiter was the first to give an idea about the classification of nano structured materials in 1995, Skorokhod further explored this idea in 2000 [1, 2].

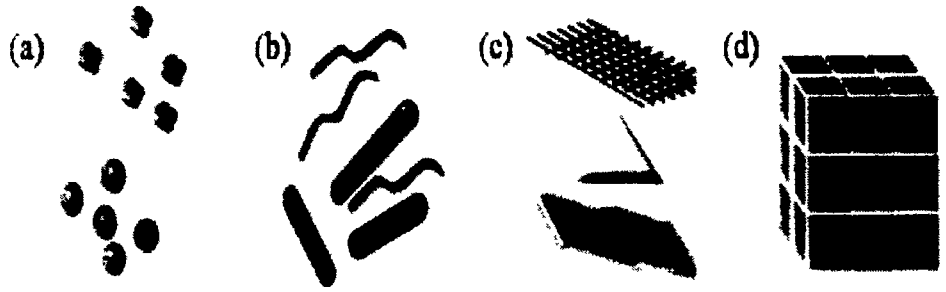

Fig. 1.1: Nano based materials: (a) 0D, (b) 1D, (c) 2D and (d) 3D [2].

1.2.1 Zero Dimensional Nano Structured Materials (0D NSMs)

Dimension wise classification of nanostructured materials shows that if all the dimensions of a material are less than 100 nm then it placed in 0D NSMs. There is no degree of freedom else than nanoscale in all dimensions. A significant progress has been made in the field of 0D NSMs in the past few years because of their intrusting practical applications in field of science and engineering. Examples of 0D NSMs are nanoparticles and quantum dots.

1.2.2 One Dimensional Nano Structured Materials (1D NSMs)

1D NSMs are those having two dimensions ranging in nano scale i.e. <100nm while one dimension is out of nano scale range i.e. >100nm e.g. nanowires, nanorods and nanotubes. 1D NSMs have novel applications in field of engineering and science. These materials have gained much attention after the key work of Iijima [3]. Examples of 1D NSMs are nanowires, nanorods and nanotubes.

1.2.3 Two Dimensional Nano Structured Materials (2D NSMs)

Dimensional wise arrangement shows that two dimensional materials are those having two dimensions not lying in nano scale i.e. two dimensions > 100 nm and one dimension < 100 nm e.g. nano films, nano layers and flower like structures.

1.3 Copper Oxide

Copper is a transition element, belongs to d–Block and Period number 4 element while oxygen belongs to P–Block and Period number 2 element in the periodic table. Copper oxide (CuO) is the binary compound of Copper and oxygen. CuO has p–type semiconductor having narrow band gap of 1.2 eV and monoclinic crystal structure [4]. It finds technological applications e.g. as pigment in ceramics to produce green, gray, pink, red blue or black glazes [5]. It is charming to researchers due to its unique properties, such as enhanced electrical

conductivity, mechanical toughness, ductility, moderate hardness, luminescent efficiency as a semiconductor. There are two well known stable oxides possible which are CuO and Cu_2O. These oxides are differing from each other due to their different physical properties i.e. different crystal structures, color, electrical properties and thermal properties. The monoclinic structure is shown in figure 1.2 which makes it interesting regarding to its properties and availability. It is nonhazardous and abundant material in the earth crust.

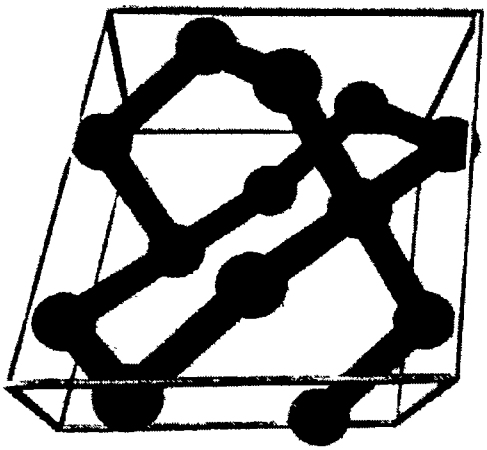

Fig. 1.2: Copper (II) oxide (CuO) crystal structure [6]

CuO is p–type semiconductor with a direct narrow band gap of around 1.2–1.55 eV in a bulk form having following fundamental properties [7];

Table 1.1: Fundamental properties of CuO bulk form at room temperature (300 K) [7-10].

Properties	Values
Lattice constants (300K)	a = 4.68 Å, b = 3.42 Å, c = 5.13 Å
Density	6.31gm/cm^3
Melting point	1975°C
Stable phase at 300 K	Monoclinic
Dielectric constant	18.1
Band gap (direct)	E_g= 1.21–1.55 eV

1.4 Copper Oxide Nanostructures

Nanostructured materials exhibit some interesting properties that are not present in bulk materials due to their high surface to volume ratio, quantum confinement effect, self purification and self alignment etc. Therefore, research is gaining rising interest in the field of nano science and technology [11].

Table 1.2: Fundamental properties of copper oxide nanostructures [12]

Properties	Values
Chemical symbol	CuO
Density	6.31 g/cm^3
Molar mass	79.55g/mol
Unit cell	a = 4.6837 Å, b = 3.4226 Å and c = 5.1288 Å
Cell Volume	81.08 Å
Cell content	4 [CuO]
Distances/ Bond length	Cu–O = 1.96 Å, O–O = 2.62 Å, and Cu–Cu = 2.90 Å

1.5 Fundamental Properties

Copper oxide nanostructures mostly appear as brownish–black powder. When it is exposed to hydrogen and oxygen at high temperature, it can be reduced to metallic copper. CuO nanostructures are more superior to micro and macro particles in their physical and chemical properties due to their massive surface areas and small size effects. Due to their promising application in different fields they have been extensively investigated by different scientists and researchers [13].

The physical properties of CuO oxides show great variation at smaller scale (nano scale) as compared to their bulk counter part because of huge surface energy and quantum size effect. It is very essential to understand the basic physical properties of CuO nano structures regarding their synthesis and applications. Crystal structure, phase transition, optical and electrical properties are the main fundamental properties to be studied in this section.

1.5.1 Crystal Structure of CuO

Tunnel in 1933 was the first to determine the crystal structure of copper oxide, after that, single x–ray method was used to further refine its structure in 1970 [14]. CuO has a monoclinic structure as shown in the figure 1.2. The number of formula unit per unit cell in CuO oxide is four. Copper atom has 4 coordination numbers, which shows that four neighbor oxygen atom are linked with it in approximately square planer configuration [15]. The lattice parameters of cupric oxide are a =4.6837 Å, b = 3.4226 Å, c = 5.1288 Å, β = 99.54° and $\alpha = \gamma = 90°$ [16]. The particle size of CuO at nano scale decreases with the increase in the unit cell volume and when the lattice symmetry try to increases the lattice constant it becomes to distorted.

1.5.2 Optical Properties

The optical properties of copper oxide nanostructures are less explored as compared to its other properties. It is reported in the literature that optical properties of copper oxide nanostructured materials strongly depend on structure, morphology, type of dopant, and synthesis technique used for its preparation.

The band gap of bulk CuO is narrow with 1.2 eV, having p–type semi conductivity. The value of the band gap is not fixed for all the structures i.e. the range of band gap of copper oxide thin film falls in 1.56 eV to 1.85 eV. The band gap of these structures is different for different structures because of quantum size effect and band tailing effect etc [17].

Several methods are employed to estimate or characterize the optical properties of nano structured materials and also to measure their band gap. UV–Vis absorption spectrometry is one of the important non destructing, quick and most convenient technique used to measure optical properties and energy structure of the semiconducting materials. Tauc calculated the value of band gap of semi conducting materials from the absorption spectrum of that material and derived an important equation i.e.

$$\alpha h\upsilon = (h\upsilon - Eg)^n \qquad 1.1$$

Here the incident photon energy is $h\upsilon$, where "n" gives information about electronic transition i.e. the transition is either direct or indirect and takes the values of 1/2 and 2 respectively, so n is called exponentional factor.

Absorption technique is the main technique used to study the optical behavior of CuO nanostructures while luminescence technique is important tool used to measure the electronic transition of semiconductors [18].

1.5.3 Electrical Properties

Electrical properties of CuO nanostructures can be measured using photo detector. Literature shows that at nano scale the electrical conductivity of CuO increases due the increase of electrons at surface. When the light is illuminated and subsequently turned on and off alternatively, the copper oxide nano structures can be switched between low and high conductors.

Three important parameters are used to measure the performance of copper oxide nano based structured materials are responsivity (R), gain (G) and detectivity (D).

For responsivity (R)

$$R\,(A \cdot W^{-1}) = I_l - I_d / P_{opt} \qquad 1.2$$

$$= \eta\,(q\lambda/hc)\,G \qquad 1.3$$

In the above equation, I_l shows photocurrent while I_d shows dark current, incident light power is shown by P_{opt} (2 $mW \cdot cm^{-2}$), and quantum efficiency indicated by η, charge on the electron is q, incident light wavelength is equal to λ (600 nm), Planck's constant is represented by h (6.6×10^{-34} J.s) and speed of light by c (3×10^{8} m/s) [19].

The ratio of the number of electrons collected and the number of absorbed photons per unit time is called photoconductive gain (G) given by

$$G = \frac{Nel}{Nph} = \tau/\tau_{tr} \qquad 1.4$$

And for detectivity (D)

$$D = A^{1/2}\,R/(2qI_d)^{1/2} \qquad 1.5$$

1.5.4 Magnetic Properties

Transition matel mono oxides (FeO, NiO, MnO and CuO) show different magnetic properties at bulk, mostly shows anti ferromagnetic behavior. The Neel temperature (T_N) of bulk copper oxide is from 213 K to 230 K and shows anti ferromagnetic behavior [20]. At nano scale, the magnetic behavior may vary from antiferromagnatic and ferromagnetic as well as to super paramagnetic behavior, which can be controlled by adjusting the bond angle between the planes of Cu–O–Cu. For example, Punnoose et al. [21] showed that there is inverse proportionality between magnetic susceptibility of CuO nanostructures and particle size. Copper oxide nano particles having size greater than 10 nm are observed to have similar magnetic properties is in bulk.

1.6 Effect of Dopants on CuO

Properties of materials are greatly depend on the dopant materials. Different dopant materials have different effects on the CuO i.e. it may change their morphology, structure, optical, electrical and magnetic properties. S. Ravi et al. synthesis Mn doped CuO due to which CuO become dilute magnetic semiconductors and also observed an increase in optical band gap [22]. Literature shows that properties of CuO nanostructures also depend on the concentration of dopant material and annealing temperature. However it needs further study in this thesis doping Mn in CuO will show significant change in its optical, electrical and structural properties which has been thoroughly discussed.

1.7 Applications of CuO

Among all metal oxides, copper oxide is an important p–type semiconductor with a narrow band gap having various important applications in different fields [23].

1.7.1 Applications in Field–Emission Display (FED)

Like other nanostructured materials, copper oxide at nano scale is usually selected as field emitters due to its high charge carrier density, low manufacture cost and low turn–on field. FED has also good color version, high clarity, less power expenditure and short response time. Copper oxide nanowires were synthesized by Zhu et al. [24] via thermal oxidation method to study their field emission properties. It was observed that copper oxide nanowires turn–on field of 3.5–4.5 V/lm and high emission current density of $450\mu A/cm^2$ at $7/\mu m$.

1.7.2 Applications in Enrichment of Thermal Conductivity of Nanofluid

Nanofluid has more thermal conductivity than traditional fluid because of its small size and Brownian motion inside the liquid, that's why it can be functional in various important fields such as airplanes, microelectronics, medicine and transportation [25]. The thermal conductivity

of non metallic solid copper oxide is reasonably high i.e. 76.5W/m k as used as additives to increase the thermal conductivity of conventional fluids [26].

Lee et al. observed that the thermal conductivity of nanofluids having particles of copper oxide nano structures in ethylene glycol is high. When average diameter of 35 nm dispersed in ethylene glycol having 4% volume of copper oxide nanoparticles, a maximum increased of 20% was observed [27].

1.7.3 Applications in Solar Cells

CuO is chosen to be one of the suitable material used in solar cells because of its low thermal emittence, simple manufacturing process, low cost and high solar absorbance. Its good electrical properties, high carrier concentration and outstanding stability make suitable in solar photo cell. CuO Nanostructured materials are used as a good absorber in solar cells technology because it is a direct way to convert solar energy into electrical energy [28].

Chandra sekaran [29] used prepared CuO nanoparticles in a solar cells which have the efficiency was about 0.863%, compared to other reported values in [30]. Theoretical efficiency value of solar cell based copper oxide nanoparticles is 20%. The record efficiency of solar cell based on CuO up to now is about 2%, so there is a plenty of space to use copper oxide in solar cell to achieve theoretical efficiency value.

1.7.4 Applications in Gas Sensors

Surface energy plays a vital role to improve the sensing properties which are potential to design high sensitivity gas sensors. Hence CuO nanostructured materials are considered as suitable material for gas sensing applications because of their high surface conductivity. Besides this, the shape of CuO nanostructures also affects the sensing properties of these materials like columnar crystal shows low sensitivity then spherical shape crystals. Also CuO

used for the detection of different compounds such as glucose, carbon monoxide and hydrogen cyanide inside a mixture.

Oroojpour et al. [31] prepared various CuO nanostructures having different size and morphologies by solvothermal route to investigate CuO sensing properties as shown in the figure 1.3. By this, they concluded that structures having low surface area are less sensitive limit and structures having high surface area have better sensing response. Thus CuO at nanoscale exhibit good sensing properties.

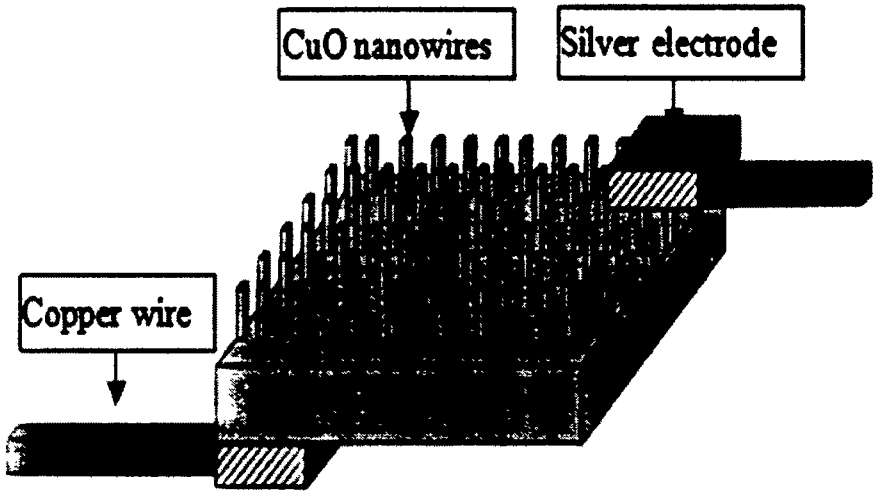

Fig. 1.3: Schematic diagram of a gas sensor based on prepared CuO nanostructures [32].

1.7.5 Applications in Lithium Ion Batteries (LIBs)

The demand of high storage medium (capacitors) is raised rapidly, so pseudocapacitors are new and attractive to researchers due to their effective properties such as excellent reversibility, long life time and power density. The ideal electrode materials for pseudocapacitors are transitions metal oxide and due to favorable pseudocapacitive characteristics CuO is one of the most suitable materials among all matel oxides. It is proved that the specific capacity was remarkably affected by particle size and morphology of CuO. M. Zhang at el. [33] synthesized nanobelts shaped, feather like and cauliflower like nanocrystals by simple chemical deposition

method. Using CuO nanostructures as an electrode material, it was noticed that morphology is greatly effect on the electrode materials of the overall electrochemical properties. Nanobelts and feather–like nanostructures have lower utilization efficiency and efficient property for electrolyte diffusion as compared to cauliflower like structure of CuO.

1.8 Aims and Motivations

Transition metal oxide nano materials are gaining much attention because of their practical applications and having unique chemical and physical properties which are greatly dependent on the morphology and size.

The aim of this research work is:

- To synthesis undoped and Mn doped CuO nanostructure using simple wet chemical method (co–precipitation).
- Successful doping of Mn cation to host matrix having single phase.
- Adjusting of different synthesis parameter to achieve different copper oxide nano structures having control morphology and uniform size distribution which are expelled to have improved physical properties.
- Tune the dielectric properties of CuO with doping to make it potential for applications.

Different parameters of the prepared Nanostructured can be investigated using characterization techniques i.e. X-Ray Diffractometry (XRD), Scanning electron microscopy (SEM), Fourier Transform Infrared spectroscopy, UV- Vis spectroscopy for its optical properties and LCR meter.

CHAPTER NO: 02

LITERATURE REVIEW

Zhong-shan Hong at el. [35] prepared CuO nanoparticles using simple alcohothermal method using copper acetate as a starting material. The prepared sample was collected through centrifugation and washed with distilled water and ethanol. A black powder was finally collected after drying the sample at room temperature. For comparison, different samples of the same material were prepared at various temperatures i.e. 90°C, 130°C, 150°C and 180°C. The prepared sample was then characterized by XRD, which showed that 3–9 nm stable CuO nanoparticles were prepared as shown in figure 2.1.

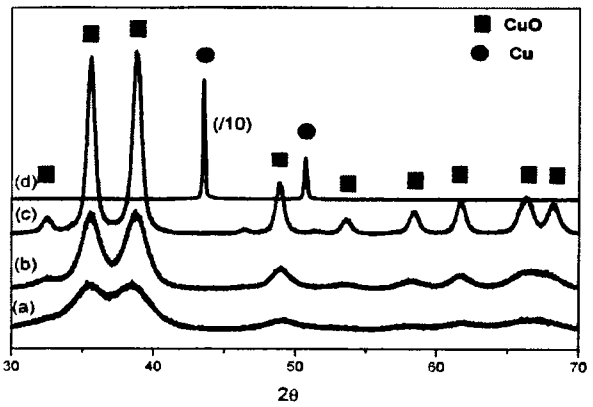

Fig. 2.1: XRD patterns at different temperatures (a) 90°C (b) 110°C (c) 150°C (d) 180°C [35]

XRD analysis showed that the size of prepared CuO nanoparticles greatly depends on the reaction temperature. By varying the reaction temperature; the change in the particle size of CuO nanoparticles were recorded. Remarkable changes occur when the reaction temperature was reached to 180° C. The prepared sample was then characterized by SEM which showed that sample is a combination of non-aggregated spherical particles. SEM analysis also reaveled that

average particle size of the prepared CuO nanoparticles is approximately equal to 11nm which justify the XRD result.

Sawsan Al–Amri at el. [36] used a surfactant free sol gel chemical technique for the preparation of Ni doped CuO nanostructures. In this process, they dissolved Cu $(NO_3)_2.3H_2O$, Ni $(NO_3)_2.6H_2O$ and citric acid in distilled water with a molar ratio of 1:1 between metal nitrate and citric acid. To remove the impurities, the prepared sol was then centrifuged and washed by ethanol for about 2–3 times. After washing and cleaning, dense black precipitates were collected. Heat treatment of the sample was carried out in electric oven for about 10 min at 200°C. Crystalline phase of pure and Ni doped CuO nanostructures were obtained by grinding and further annealing at 350°C.

Crystallite size was calculated from the XRD pattern using Debye Sherrer's formula which was in the range of 23 to 47nm, while the sharpness of peaks indicated that pure single phase highly crystalline structure was formed. Raman spectroscopy was done to analyze the arrangement of atoms and vibrational modes of Ni doped CuO nanoparticles prepared by sol–gel technique which also explained the formation of pure and Ni doped CuO nanoparticles having no contamination of Cu_2O. It was also concluded from Raman spectroscopy that, fundamental peak shifted toward lower wave number by increasing the concentration of dopant element i.e. Ni because of the reduction of particle size. UV–visible analysis conformed that band gap increased by dopant element (Ni), because of the quantum size effect of the semiconductors.

Neupane et al [37] used hydrothermal synthesis route for the synthesis of CuO nanoparticles by controlling the reaction temperature between copper nitrate trihydrate and sodium hydroxide. XRD and SEM results indicated a flake like morphology of CuO nanoparticles with uniform size distribution between 3–7 nm. It was conformed from the series

of experiment that reaction temperature and partial pressure inside an autoclave greatly affect the morphology of CuO nanoparticles. In order to explain the morphology variation as a functional temperature, another experiment was conducted by the same group by fixing the reaction time for 2 hours and varying reaction temperature. Impurities like Cu_2O and $Cu(OH)_2$ were appeared for lower temperature i.e. 100°C, while for higher temperature i.e. 300°C pure monoclinic phase structure of CuO nanoparticles was observed. For hydrothermal method, it is very important to tune the reaction temperature according to the desired morphology.

Tariq Jan et al. [38] prepared CuO nanostructures doped with Sn by simple co–precipitation technique using copper chloride and sodium hydroxide as precursors. Anti cancer activity and different physiochemical properties were investigated using various characterization techniques. Peaks and width pattern obtained from XRD illustrated the formation of nano particles having monoclinic structure. SEM analysis of Sn doped CuO nanostructures indicated that rod morphology significantly change to simple particles as a function of doping concentrations. Raman spectroscopy was done for further analysis of the defects and microstructure properties of nanomaterials which indicated the formation of pure monoclinic crystal structure of CuO. Optical properties of the prepared samples were investigated by UV–visible spectroscopy which illustrated those absorption peaks of the prepared CuO nanoparticles reduced with Sn doping, while the crystallite size gradually decreased as the amount of Sn increases. The band gap recorded from UV-Vis spectroscopy revealed the decreasing trend from 2.83 to 2.09 eV for undoped to 10% Sn doped CuO nanostructures due the band tailing effect.

Joon Kang at el. [39] prepared CuO nanowires of 90 nm diameters and of several hundred nanometer lengths (with and without TG) using simple wet chemical technique. The precursors used for the typical experiment was copper acetate [$(CH_3COOH)_2$ H_2O] and sodium hydroxide

[NaOH]. The morphology of prepared CuO nanostructures was investigated by XRD and SEM analysis. XRD peaks showed that the prepared CuO nanostructures have monoclinic structure and have no characteristic peaks of impurities and other elements. While SEM showed the influence of organic molecules TG on the morphology of prepared CuO nanostructures. FTIR spectrum was recorded in the range of 400 to 4000 cm^{-1} having three characteristics peaks at 432 cm^{-1}, 497 cm^{-1} and 603 were observed for prepared CuO nanostructures. Without TG formation suggested a CuO flower like nanostructures having individual nanowires were present while isolated CuO nanowires were obtained in the presence of organic molecule TG.

Mohammad Azhar et al. [40] successfully synthesized one dimensional CuO nanorods using simple hydrothermal route having copper acetate and hexamethylamine (HMTA). X–ray diffraction showed the peak for pure monoclinic crystal of CuO nanostructures. SEM analysis of the prepared samples showed agreement with the XRD results and formation of uniform sized nanorods.

R Al Gaashani et al. [41] used thermal decomposition method for the preparation of CuO rice like nanostructures from copper nitrate under different conditions. The morphology and size ware controlled by varying decomposition time and temperature of the process. The size and morphology of the prepared nanostructures was investigated by XRD followed by SEM. The results suggested that morphology showed direct variation with reaction temperature i.e. increasing the reaction temperature causes increase in the crystal size. The UV–Vis result illustrated that the band gap decreased with increasing as a function of reaction temperature in fix time due to the increase in the crystalline size. XRD result for a quick, inexpensive and simple

method proved the formation of rice like morphology having monoclinic crystalline phase of CuO supported by SEM analysis.

Electrochemical and deposition process were used by Buppachat Toboonsung at el. [42] to synthesize CuO nanorods and their bundles on glass substrate. Morphology and thickness was optimizing by deposition time, electrode separation and applied voltage. Aggregation mechanism was used for the formation of nanorods and their bundles. It was noticed that the annealing temperature affected the transformation of Cu phase in as deposited sample to a single CuO phase. Crystallinity and grain size growth in the annealed sample are found to be responsible for increasing in photoluminescence intensity.

Tariq Jan et al [43] used simple Co–precipitation method for the formation of cerium (Ce) doped CuO nanostructured materials. XRD analysis of the prepared doped and undoped samples indicated the formation of monoclinic crystal structure. SEM results indicated that morphology changed from nanorods to nanosheets by changing dopant concentration as well as gradual increase in the thickness occurs with increasing dopant concentration. FTIR results also supported the previous results obtained from XRD and SEM analysis. UV–Visible analysis showed that undoped CuO weakly absorbs the light in visible region and strongly in ultra visible region.

Simple chemical precipitation method was used by Hongxia Zhang at el [44] to prepare the flower like CuO nanostructures for electrode materials. Two different solutions were prepared using copper nitrate Cu $(NO_3)_2$, hexamethylenetetramine $(C_6H_{12}N_4)$, and polyethylene glycol, $Cu(NO_3)_2$, with different concentration of PEG. The prepared samples were then characterized using XRD, which reflected to the monoclinic structure of CuO nano flowers. The peaks also indicated that there were no impurities of other oxide e.g. Cu_2O. SEM analysis also

supported the results obtained from XRD, and spherical as well as circumferential symmetries were observed depending on the concentration of PEG. It was clear from the electrochemical properties that tuning the morphology increases the specific capacitance of CuO i.e. higher the surface area results high specific capacitance.

Mahdi Shahmiri at el. [45] prepared CuO nanosheets using simple precipitation method and studied the effect of pH on it. It was confirmed from the XRD study that size and shape greatly depend on the pH value. CuO nano structures were obtained only at higher pH values, while for lower concentration of NaOH, the reaction did not complete hence no formation of CuO nanosheets occur. SEM analysis also supported XRD results illustrating that CuO nanosheets have been formed at higher pH values.

Ibrahim Y. Erdogan et al. [46] prepared CuO flower like nanostructure using spin coating and annealing temperature on substrate. The prepared nanostructures were then characterized by XRD, FTIR and UV–Visible spectroscopy. Structural results obtained from XRD suggested the formation of single phase monoclinic crystalline structure which was supported by FTIR analysis as well. The band gap of CuO nanostructure was found to be 2.64 eV as measured by UV–Vis analysis.

Yunling Zou et al [47] used $CuCl_2 \cdot 2H_2O$ and NaOH as precursors for the fabrication of flower like CuO nanostructures in the presence of CTAB which was used as a surfactant by simple hydrothermal route. Width and peak intensity obtained from XRD indicated that the samples were pure monoclinic structure and nanocrystalline nature. Morphology of prepared samples was investigated by SEM which indicates the formation of flower like CuO nanostructures interconnected by nanosheets of width up to 60–80 nm and length up to several nano meters.

S. Harish et al [48] performed series of experiments to prepare porous CuO nano spindles like structure without any use of template. Length of the prepared samples was about 150 nm while the average diameter was about 70 to 80 nmMonoclinic phase of CuO nanostructures shown by intensity peaks obtained from XRD. SEM results illustrated that the reaction concentration greatly affected the morphology of the obtained structure which changes from nanospindle like particles to nanospindle sheets by varying the reaction concentration. The prepared samples showed an increasment in the band gap from 1.7eV to 2.5eV for different copper acetate solution. The increase in the band gap refers to quantum confinement effect from nanospindle to nanosheets.

CHAPTER NO: 03

SYNTHESIS AND CHARACTERIZATION TECHNIQUES

In order to understand the potential applications of nanotechnology, it is very necessary to have the ability to process and fabricate the nanostructures materials. The main objective of researchers is to control size, shape and crystallite structure of nanostructured materials regarding their practical applications in various fields including medicine, electronics and catalysis. Hence Bottom–up and top–down are the two important tools used for the fabrication of nanostructured materials.

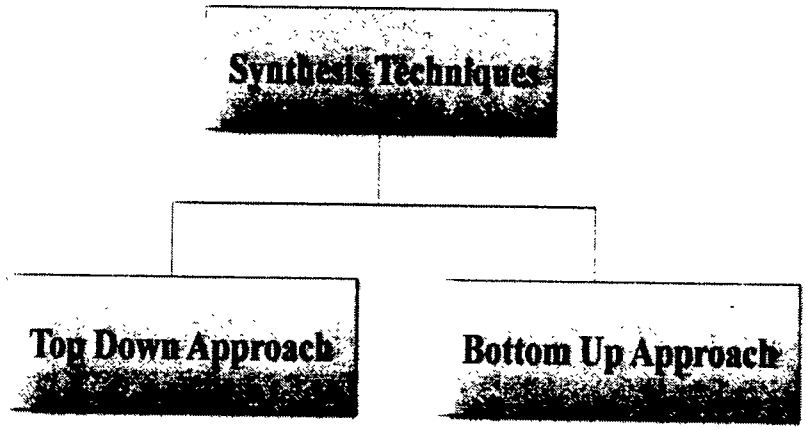

Fig.3.1: Blog Diagram of Synthesis technique

3.1 Top–Down Approach

Top down approach is one the traditional approach used to break down the bulk materials into micro or nano scale according to their practical applications. Important top down approaches includes ball milling, lithography, chemical and dry etching. This approach is generally low cost, efficient and advantageous for integrated circuits (ICs) [49].

However it is very challenging to control the morphology and size of materials synthesized by top–down approach e.g. nanowires fabricated through top–down approach are not enough smooth and pure.

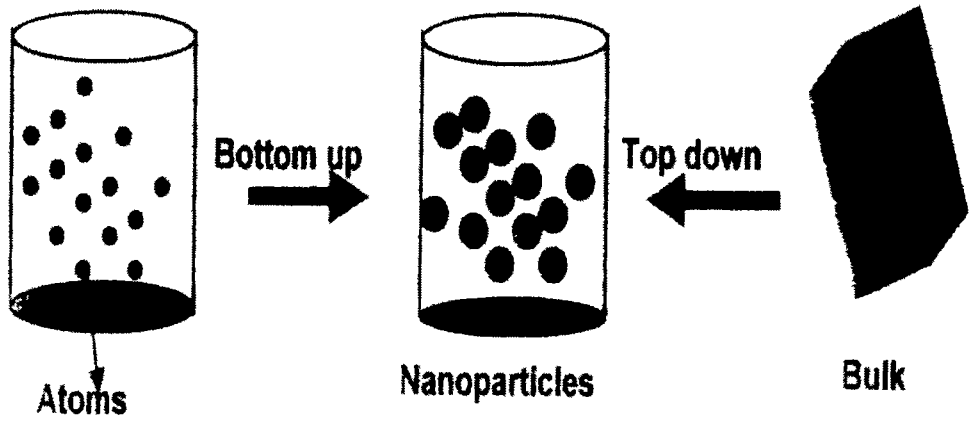

Fig. 3.2: Schematic diagram of Top–down and Bottom-up approach [49].

3.1.1 Lithography

Lithography is an important tool used to get smaller size by which image is to be printed with wax or oil on a flat smooth surface. At gives great strength, performance, low energy consumptions and cost as going towards smaller and smaller size. Various lithographic techniques such as optical lithography, electron beam lithography and x-ray lithography are used for fabrication of devices at nanoscale [50, 51].

3.1.2 Ball Milling Process

Ball milling is one of the important technique among all top down approaches used for the synthesis of different nanostructured materials, nanocomposites, and nano-alloys [52]. The particle size of appropriate dimensions is reduced and converted into new phases by placing it in a high energy mill. The ball rolls down freely on the materials inside closed chamber crushing

the bulk powder at nanoscale as shown in figure 3.3 [53]. Ball milling process is more economical for the production of large scale nano size materials. This technique is limited for the production of uniform size nano structure of materials with uniform size [54].

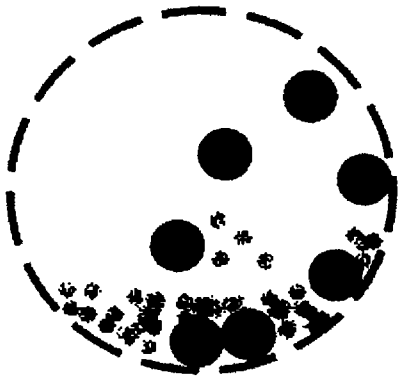

Fig. 3.3: A typical ball milling chamber [54]

3.2 Bottom Up Approach for Nano Structured Materials

An alternative approach which has the potential of creating more economical and less raw materials is the 'bottom– up' approach. In this approach the materials are suggested to build up from the basic i.e. molecule–by–molecule or atom–by–atom making self assembling. This approach is much effective due to very small structure defects, low cost and easy control [55, 56].

3.2.1 Chemical Vapor Deposition (CVD)

Chemical vapor deposition is the process through which volatile precursors are transported through vapor phase to the reaction chamber to adsorb on a heated substrate. A high temperature i.e. above 900°C is required to start a reaction in thermal CVD, while plasma CVD reaction is started in the temperature range between 300 and 700°C.

It is widely used in thin film coating to a suface, materials–processing technology and high quality bulk materials. The main advantage of this method is that, film prepared through

this process has uniform small size thickness. While the main drawback of this method is the precursors which are used in this method are volatile at room temperature. May elements in the periodic table cannot fill this requirement therefore it is more often retracted to metal organic precursors [57]. Main steps involves in this method are broadly shown in figure 3.3.

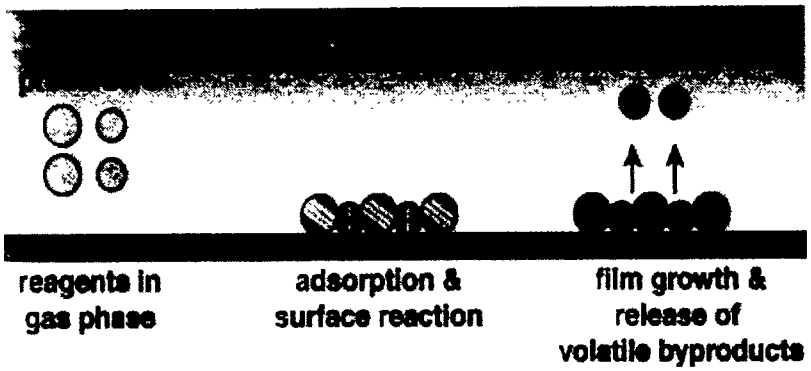

Fig. 3.3: Schematic diagram of Chemical Vapour Deposition (CVD) process [58]

3.2.2 Physical Vapor Deposition (PVD)

It is a technique used for the preparation of thin films of different materials on various substrates in the presence of vacuum. The desired pattern can be easily transferred to the substrate through this method. Reaction in PVD is completed at lower temperature as compared to CVD which make it more convenient. Also this method consists of various types .i.e. evaporation, sputtering and molecular beam epitoxy [59].

3.3 Wet Chemical Method

Wet chemical method is one of the most common and effective bottom up method used for the preparation of MO nanostructures with require control of size, shape and composition. It is usually suitable for large production and requires low reaction temperature. Size, shape, dimensions and composition of desired structure can easily be controlled entire process through this method [60 –62].

This technique consists of following sub techniques.

- Hydrothermal process
- Sol gel process
- Coprecipitation method
- Electrodeposition method
- Template base synthesis
- Nucleation and oriented attachment

3.3.1 Hydrothermal Process

Hydrothermal process is one the most promising method used for the development of very small size crystal growth for verity of technological applications. Hydrothermal is the combination of two Greek words "hydro" meaning water and "thermos" meaning heat. It is the process in which water is used as solvent for any heterogeneous reaction under high pressure and temperature to dissolve materials that insoluble under ordinary conditions [63]. Reaction is usually carried out in a pressurized sealed container below 250°C.

In the recent years, hydrothermal process is not limited to crystal growth of nanomaterials but several interdisciplinary branches of science also covered by its broad range. Hydrothermal process is carried out in a reaction vessel known as autoclave. Highly corrosive solvent at high pressure and temperature for longer time must be supported by an autoclave. This method is much effective for the synthesis of various nanostructures like nanospheres, nanorods, nanoflakes and nanowires etc having different properties depending upon the solvent used in it [64].

3.3.2 Sol Gel Synthesis Technique

Sol gel is an important two step process used for the synthesis of nano structured material from solution. The first important step is the formation of colloidal suspension known as sol

while in the second step hydrolysis and polymerization of molten precursors occur to convert it into irreversible gel. An important parameter in this method is the selection of suitable metal precursor used for the formation of polymeric gel. Viscosity, temperature, pH and solvent are the various factors effecting nanostructures prepared through this method [65]. The main advantage of this method is to control the chemical reaction parameters which able to control the final structures of products.

3.3.3 Coprecipitation Method

Simple and important chemical method used for the fabrication of nanostructured materials by the precipitates of substances soluble under suitable conditions. Chemical reaction, nucleation and crystal growth are the three important steps of chemical co-precipitation method. Nucleation plays important role in this technique in which ions, atoms or molecules combined together in a definite pattern to form a characteristic solid. Due to nucleation an additional particles may deposited on the desired nanostructure which further affect the size and morphology of that structure. Precursors used in this method are mostly soluble in easily available solvent i.e. water [66, 67]. Mostly, high degree of suspension, uniform spatial concentration distribution inside a reactor and uniform growth time for all crystals or particles are most essential part to control in this method to gain nanostructures with narrow size distributions. To form a homogenous solution mostly inorganic salts (chloride, sulfate, nitrate etc.) are used as a precursors so that they can be easily dissolved in water.

3.3.3.1 Advantages of Coprecipitation Method

Following are the advantages of this method

- Highly pure nanocrystals can be easily prepared
- Size of the nanocrystals can be 35–40 nm prepared through this technique

- The other important advantage of this is that both aqueous and non aqueous medium can be used

Undoped and Mn doped CuO nanostructures can be synthesized in the present work following the discussed method.

3.4 Experimental Procedure of Thesis Work

Different precursors are used for the preparation of CuO nanostructures in this thesis.

- Distilled water, as reaction medium (solvent).
- Copper chloride ($CuCl_2.2H_2O$)
- Manganese chloride ($MnCl_3.2H_2O$)
- Acetic acid (CH_3COOH) used as a surfactant for controlling the particle size.
- Sodium Hydroxide (NaOH) used to adjust pH values,

Undoped and Mn doped CuO nanostructures have been prepared using simple coprecipitation method. To obtain 1%, 3% and 5% Mn doped CuO nanostructures, a proper ratio of copper chloride dihydrate ($CuCl_2 \cdot 2H_2O$) and Manganese chloride ($MnCl_3.2H_2O$) has been dissolve in distilled water. Sodium hydroxide used to the adjusted the pH value of prepared solution up to the desired limit. Acetic acid (CH_3COOH) has been used as a surfactant to control the size and restrict the particle from agglomeration.

0.1M solution of copper chloride dihydrate ($CuCl_2.2H_2O$) and $MnCl_3.2H_2O$ has been obtained by dissolving them into 100 ml distilled water. The solution has been magnetically stirred for 10 minutes at 500 rotations per minute (rpm). After 10 minutes of stirring, ionic surfactant i.e. acetic acid has been added to the solution. Addition of surfactant is important to control the agglomeration of the particles. After 10 minutes, pH value has been adjusted by the addition of NaOH drop wise to the stirring solution which also results in the nucleation of

particles. The drop wise addition of NaOH stopped once the pH level reaches above 10 and the solution become weak basic. To complete the reaction, it has been set on the hot plate at 100°C, and stirring at 500 rpm for 1 hour. When the reaction was completed, then it was removed from the hot plate and centrifuged to wash the solution by distilled water for several times. In order to dry the solution, it has been kept in the electric oven at 80°C for overnight. A black powder has been obtained on the next day which was further dried and grinded. The prepared samples have been annealed for 3 hours at 300°C to enhance the crystallinity. Same method has been repeated for 1, 3 and 5 % Mn doped except to addition of different amount of manganese chloride in various molar ratios.

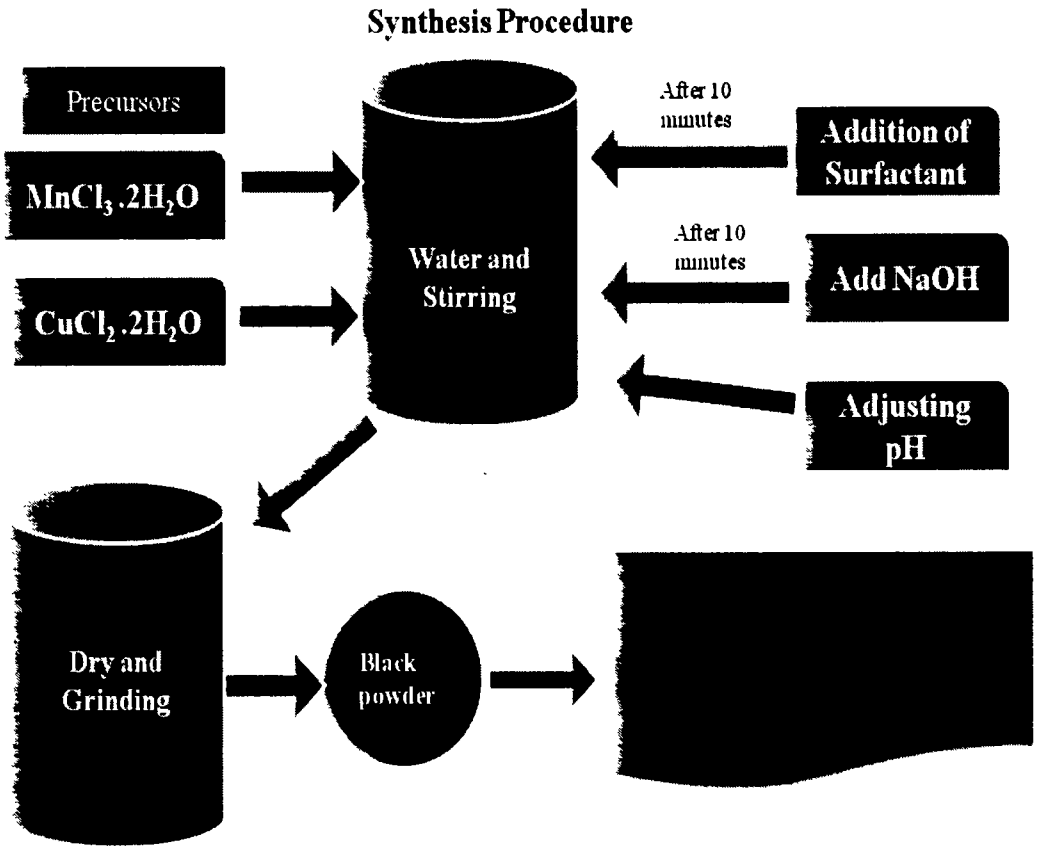

Fig. 3.4: Flow chart of synthesized samples

3.5 Characterization Techniques

Characterization is an important step to obtain all the required information from the samples. Information about different physical properties (electrical, optical, structure and chemical etc) can be gained through different characterization techniques. An effort is done in this thesis to study different physical properties i.e. structural morphology, chemical, optical and electrical using various characterization tools.

3.5.1 X–Ray Diffractometry (XRD)

X–ray diffraction (XRD) is the important technique used for the determination of crystal structure and its related parameter included grain size and lattice constant etc. This tool is supposed to be fingerprint for structural investigations of crystalline materials. Three dimensional atomic distribution leads to the formation of crystal lattice. So parallel planes are formed by the series arrangement of these atoms, the planes are separated from each other by a small distance "d". This spacing varies for material to material indicating that each material has its own characteristic d– spacing. X–rays are scattered to certain manner due to the interatomic distances which is comparable to the wavelength of the incident x–rays.

3.5.1.1 Working Principle

The basic working principal for XRD is Bragg's law of diffraction. Pure crystalline solids have repeating units of atoms in regular order. When a series of equally spaced parallel planes comes on the way of x–rays it reflects from them with a path difference $2d\sin\theta$. For constructive interference, this path difference is equal to $n\lambda$. From figure 3.5 the mathematical form of Bragg's Law can be written as [68].

$$2d\sin\theta = n\lambda \qquad 3.1$$

Where

d = interatomic spacing

θ = angle between incident ray and surface of crystal

λ = wavelength of the incident x–rays

n = integer

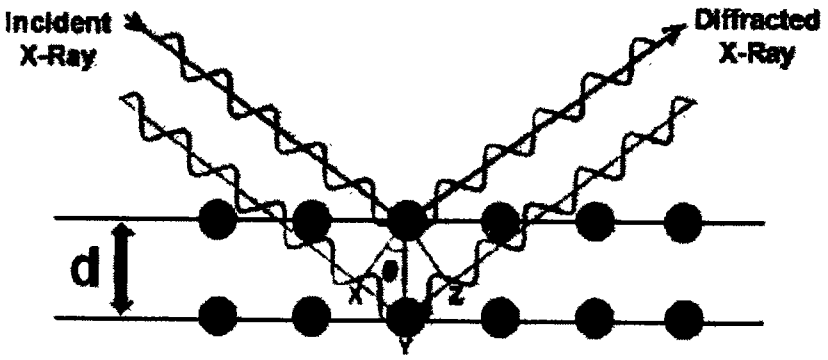

Fig. 3.6: Schematic illustration of the x–ray diffraction by crystals [68].

Crystallite size of any materials can be found using Scherer's formula. Crystallite size is calculated by selecting the full width at half maximum (FWHM) from the peak of maximum intensity. The formula given below is used for calculating crystalline size through Scherer's formula.

$$D = \frac{k\lambda}{\beta \cos\theta} \qquad 3.2$$

Where

K = constant,

λ = is the wavelength of x–rays which is equal to 1.504 Å in case of CuK_{α},

β = the full width at half maximum

θ = angle of diffraction [69].

3.5.2 Field Emission Scanning Electron Microscopy (FE–SEM)

Field emission scanning electron microscopy (FE–SEM) is a tool used to explore the topography, morphology and material composition of the sample. It is more convenient than optical and conventional scanning electron microscopes because of its high resolution power. A beam of high energy electrons scan the surface of the sample. Tungsten LaB_6 (lanthanum hexaboride) filament is heated in conventional electron microscope to produce a beam of electron, while in FESEM ,field emission electron beam is used.

3.5.2.1 FESEM Working Principle

In conventional scanning electron microscopy, hot electrons are produced by heating the filament, while in FESEM, strong electric field produces cold electrons from the conductor's surface. SEM is used to obtain the images of sample surface with high resolution. A very thin tip of tungsten having diameter in the range of 10 to 100 nm is used in FESEM as an electron gun. Electronic lenses are used to focus these field emitted electrons in a zigzag path to scan the sample surface. Ultra vacuum of 10^{-6} Pa for microscopic column along with the acceleration voltage in the range from 0.5 to 30 kV is required between anode and cathode for FESEM to operate [70] as shown in figure 3.7.

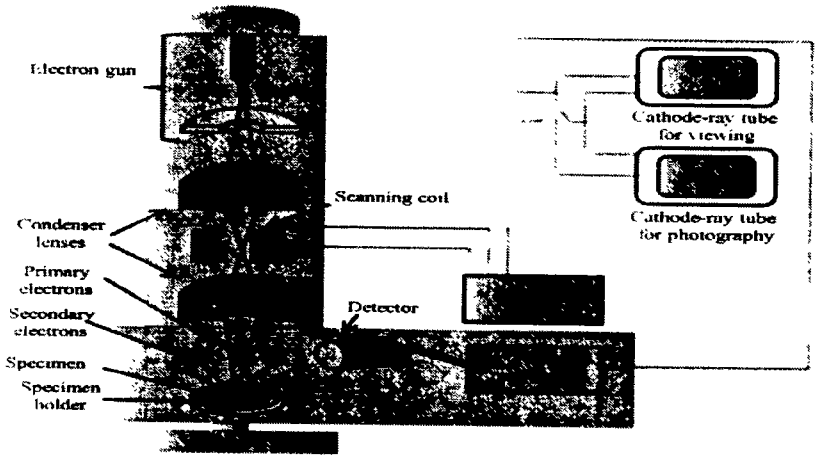

Fig. 3.7: Schematic diagram of FE–SEM [70].

Various types of signals i.e. secondary electrons, x–rays and backscattered electrons etc are emitted after the striking of primary electrons with the sample surface are detected by signal detector [71]. Figure 3.8 shows the interaction of electrons with the sample and the production of various signals.

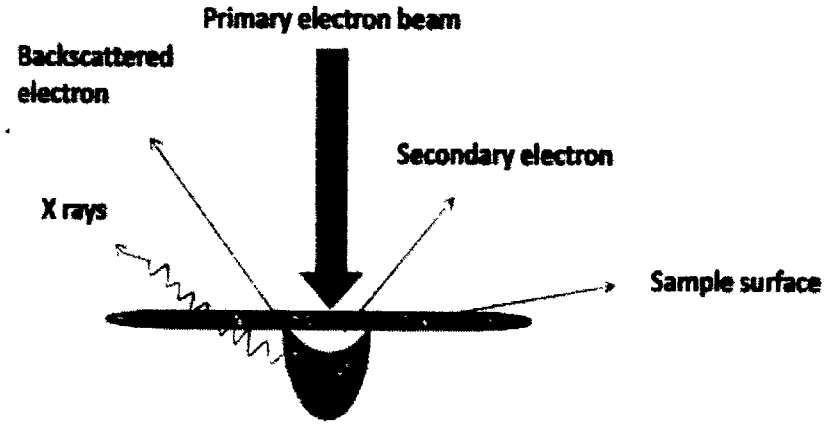

Fig. 3.8: Schematic diagram of specimen–electron interaction [72].

Secondary electrons among these generated signals are responsible for morphological analysis by the detector which converts these signals into electronic signals. For further process and future work these signals are amplified, saved and converted into image which can be seen on the monitor. Before FESEM analysis, non–conducting samples are converted into conducting by carbon or gold coating.

The quality of FESEM image is much better than that of optical and conventional SEM because the electron beam generated by field emission is 1000 times smaller than the others. Therefore, in the field of nanotechnology, FESEM is very useful tool for high resolution morphological investigation [73].

3.5.3 Energy Dispersive Spectroscopy (EDS)

EDS is an important tool for the characterization of chemical compounds. It is based on the idea that each and every atom can generates x–rays of its own spectrum and nature because every single atom has its own characteristic structure as shown in figure 3.8 [74].

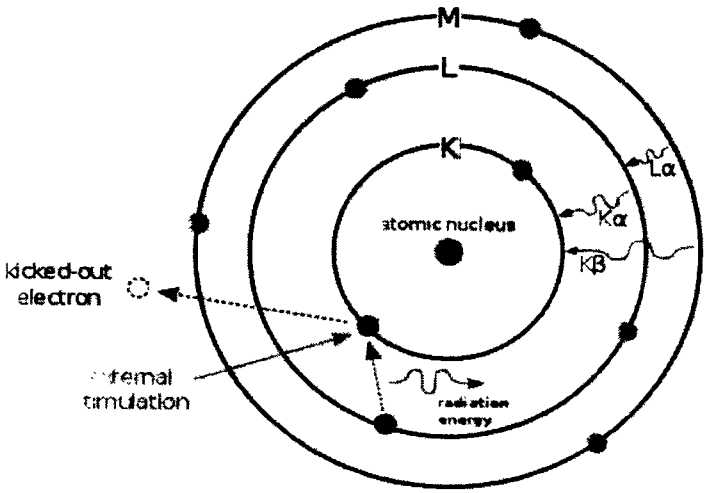

Fig. 3.9: Schematic diagram of EDS mechanism [74].

3.5.3.1 Working of EDS

Due to inelastic collision, inner shell electrons can be removed by the incident beam. As a result, holes are generated in these inner shells which are filled by electrons from the outer shells. While moving from high energy level to low energy level, these electrons lose some energy in the form of x–rays of its own wavelength and energy. EDS is useful in sense that it can be carried out in area of different sizes, at a specific spot or across the sample surface.

3.5.4 Fourier Transforms Infrared Spectroscopy (FTIR)

Interaction between electrons and the outermost orbits holds the atoms at a certain distance in a material. By taking energy, these atoms vibrate about their equilibrium point through electromagnetic energy. The vibrational properties of chemical bonds present in a

material are determined by infrared analytical tool. It is also used for detection of extra elemental components in the sample, unknown material and also for quality of sample. The quantum number for an atom describes that vibrational energy is quantized and has only certain values. Therefore each material has its own IR spectra because it is composed of unique atoms [75]. The basic model of FTIR spectroscopy is shown in figure 3.9.

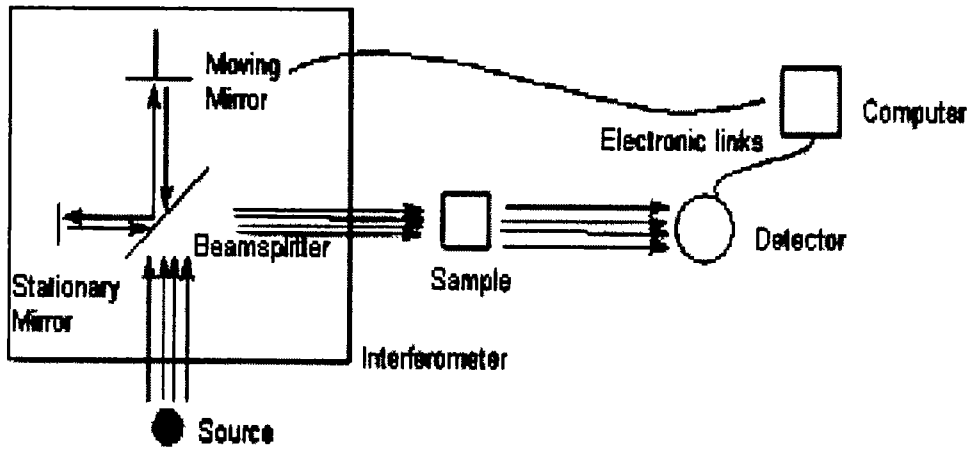

Fig. 3.10: FTIR spectroscopy [75]

3.5.4.1 Working of FTIR Spectroscopy

Black body source is used for generation of infrared energy beam. The energy required to the sample and ultimately to the detector is controlled by passing it through an aperture. The beam inters the interferometer which produces a unique type of signals which has all of the infrared frequencies encoded into it. An interferometer use beamsplitter which collects the incoming infrared beam and divide it into two optical beams. One beam is reflecting off by flat mirror which is fixed and the other is reflected off by moving mirror. Both these beams reflected from their respective mirrors and recombined at the back of beamsplliter and generate a signal from samples called as interferrogram. This interferrogram has unique property for every signal

point from the mirrors, thus gives information about every infrared frequency that come from the source [76].

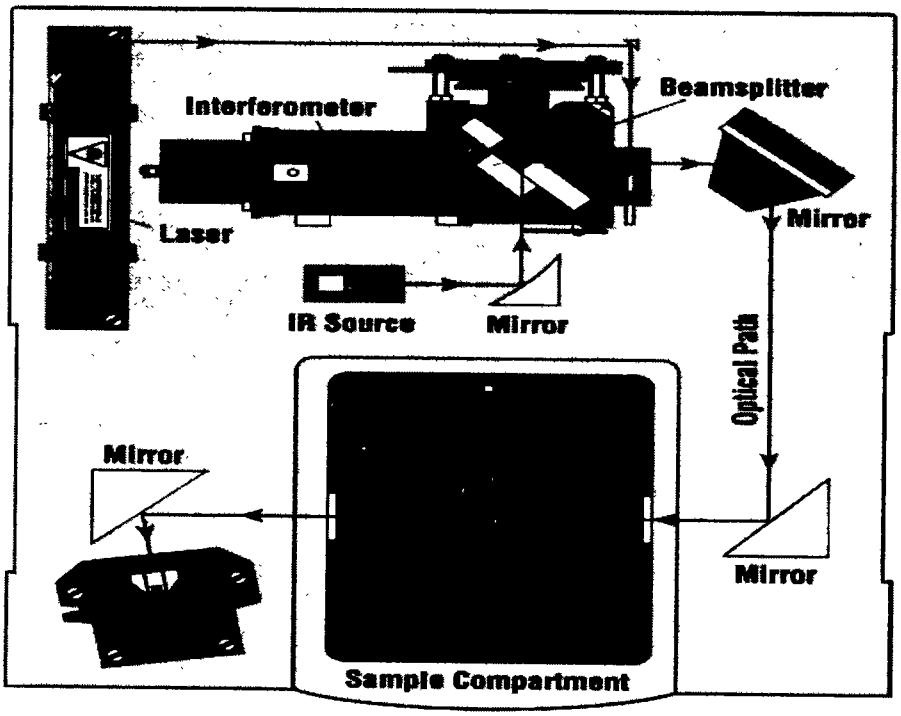

Fig. 3.11: Schematic diagram of Fourier Transform Infrared Spectroscopy (FTIR) [76]

3.5.5 Ultraviolet (UV) Spectrophotometery

Ultraviolet (UV) spectrometry is one of the important tools used for the quantitative study of electromagnetic spectra. Its basic function is to produce light in UV and to calculate the spectrum of light reflected, transmitted and absorbed by the sample. Figure 3.12 shows basic components of UV-Vis spectroscopy.

The two major functions performed by this device are.

i. Generate light in visible region which sticks with the sample.

ii. Calculated the spectrum of light reflected, absorbed and transmitted through sample.

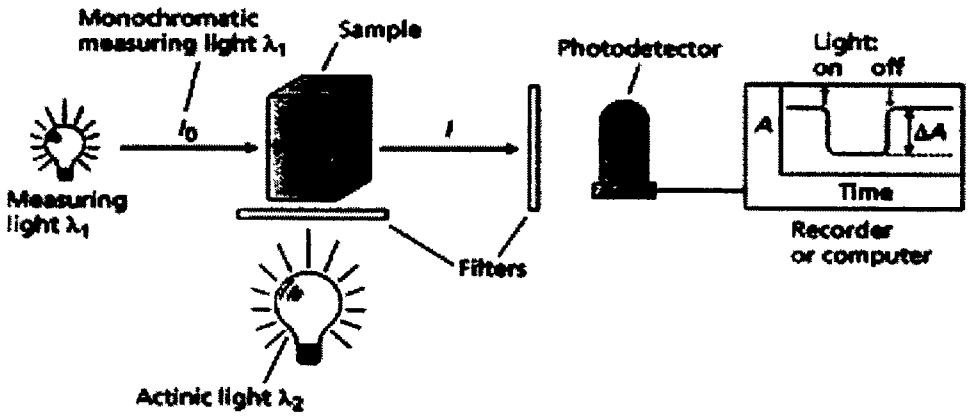

Fig. 3.12: Schematic diagram of spectrophotometer [77].

3.5.5.1 Working Principle of UV Spectroscopy

A continuous spectrum of wide band gaps is generated by spectrophotometer. This spectrum is collected by monochromator which allows only one color and passes it direct to the sample. After passing through the sample, intensity of the transmitted light is measured using photometer. Three possibilities as shown in figure 3.12 may occurs in light samples interaction e.g. the light may, reflect (R), absorb (A) or transmit (T) [78, 79].

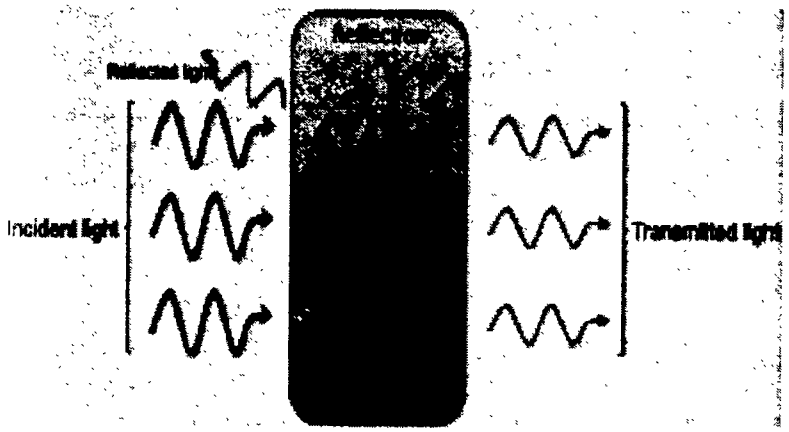

Fig. 3.13: Schematic illustration of the main mechanisms affecting the transparency of a material [79].

Mathematically it is written as

$$R + A + T = 1 \qquad 3.3$$

The light transmitted through the sample has intensity "I", than transmission in term of intensity is written as

$$T = \frac{I}{I_0} \qquad 3.4$$

Absorption is written as

$$A = -\log 10\,(T) \qquad 3.5$$

$$\text{As} \quad T = \frac{I}{I_0} \qquad 3.6$$

Therefore

$$A = -\log 10\,(I/I_0)\; A = -\log 10\,(I/I_0) \qquad 3.7$$

If the initial absorption edge of sample corresponds to wavelength λ_1 then the wavelength which is greater than λ_1 will be transmitted from the sample and vice versa if the wavelength is less than or equal to λ_1.

3.5.6 Dielectric Measurements

LCR (inductance-capacitance-resistance) meter is an important tool used to measure the dielectric properties of the samples. There are two main types of LCR meter i.e.

- Handheld LCR meter which has normally adaptable frequencies up to 100 kHz and
- Benchtop LCR meter which has adjustable test frequencies higher than 100 kHz.

An AC voltage is applied to the device under study (DUT) i.e. sample under study to measure the dielectric properties of any sample. In case of powder sample, pallet is made for dielectric measurements. Current passing through the sample as well as voltage present across the sample is measured by LCR meter. An advanced LCR meter is used to measure frequency dependent capacitance, inductance, impedance and resistance. Different other parameters such as

dielectric constant, dielectric loss and AC conductivity can be calculated by manipulating the measured data.

3.5.6.1 Dielectric Constant

Dielectric constant is the ratio of capacitance of a capacitor when medium i.e. insulator is placed among the plates of a parallel plate capacitor to the capacitance without medium. It is also known as relative permittivity and given by the following formula.

$$\varepsilon' = \frac{C}{Co} \qquad 3.8$$

Where " ε' " is the dielectric constant "C" is the capacitance of the capacitor when medium is placed among its plates and "C_o" is the capacitance of the capacitor without medium.

Capacitance of parallel plate capacitor is given by the relation.

$$C = \frac{\varepsilon}{Ad} \qquad 3.9$$

Where "C" is the capacitance of the capacitor, "ε" is the ratio of dielectric constant when medium is placed between the plates of the capacitor to the dielectric constant in free space. "A" is the area of the pallet and "d" is the separation between the plates or thickness of the pallet [80].

3.5.6.2 Tangent Loss

When there is no medium among the plates of a capacitor then current leads the voltage by 90^o while in case of any dielectric medium placed between the plates of the capacitor then some energy is lost due to presence of resistor or heat etc. a phase shift of ($90°$-δ) occurs among current and voltage. The dissipation or loss of this energy is named as dielectric or tangent loss which is the ratio of imaginary part of dielectric constant to the real part of dielectric constant.

CHAPTER NO: 04

RESULTS AND DISCUSSIONS

Chemical coprecipitation method as discussed earlier has been used to prepare samples of undoped and Mn doped CuO. Various characterizations i.e. x-ray diffraction (XRD), scanning electron microscopy (SEM), energy dispersive x-ray spectroscopy (EDS), Fourier transform infrared spectroscopy (FTIR) and UV-Vis spectroscopy have been used for different structural, morphological and chemical investigation respectively.

4.1 Structural Properties

Structural characteristics of synthesized undoped and Mn doped (1%, 3% and 5%) CuO samples have been investigated by XRD in 2θ range from 20° to 80° at room temperature. The obtained XRD patterns are shown in figure 4.1 which shows the formation of typical monoclinic structure of CuO (JCPD card # 9016326) having all the peaks are indexed to (110), (111), ($\bar{1}$11), (202), (020), (202), (020), (202), ($\bar{1}$13), ($\bar{3}$11) and (220) planes.

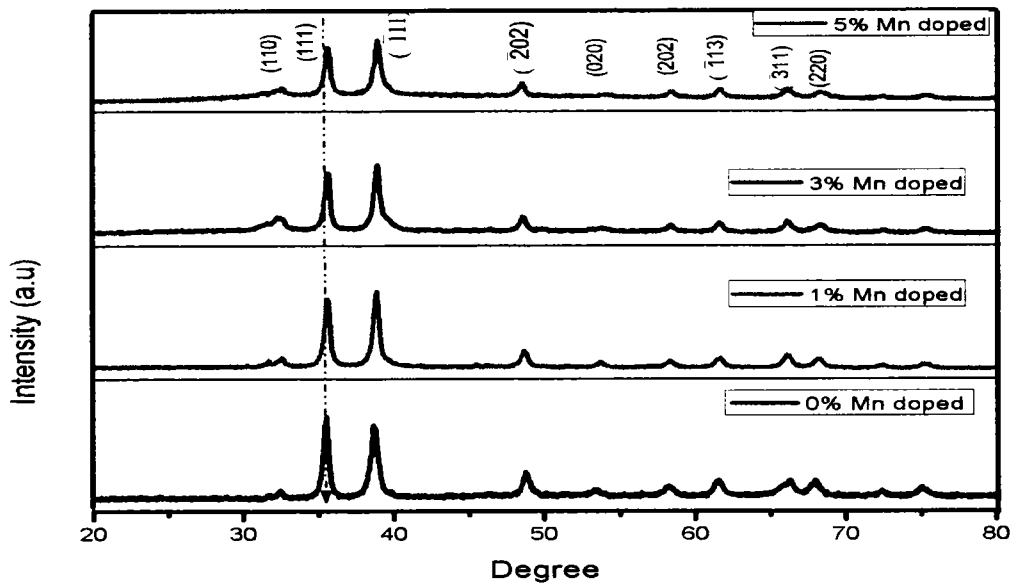

Fig. 4.1: XRD patterns of undoped and Mn doped CuO samples.

The results of XRD patterns show the formation of single phase monoclinic structure of CuO having no extra peak of Mn in the graph. It is found that dopant material (Mn) has no effect on the crystal structure of synthesized CuO. A preferred growth orientation (toward higher angle) is observed in the most intense peaks (111) and ($\bar{1}$ 11) by varying Mn doping concentrations of the prepared samples of CuO due to the decrease in the lattice parameters [80]. The XRD results illustrates that Mn ions have been replaced Cu sites without changing the basic monoclinic structure. Similar structural variations have also been observed in literature [81]. The repression and peak shift in the intensities clearly indicate the successful adjustment of Mn ions into CuO host matrix. This clearly indicates that Mn doping significantly changes the crystalline size of CuO and might be linked with the enhancement of its crystalline quality [82]. Average crystallite size has been found to be in the range of 19 to 24 nm given in table. 4.1.

Table 4.1: Value of crystallite size of all prepared samples

Sr. No	**Sample**	**Crystalline size "D" (nm)** $D = 0.9\lambda/\beta \cos\theta$
1	$Cu_{1\,00}\,Mn_{0\,00}O$	19.54
2	$Cu_{0\,99}Mn_{0\,01}O$	21.04
3	$Cu_{0\,97}Sn_{0\,03}O$	24.03
4	$Cu_{0\,95}Sn_{0\,05}O$	21.00

Debye Scherer's formula has been used to calculate the average crystallite size of the undoped and Mn doped CuO samples from the broadening of most intense peaks i.e. (111) and ($\bar{1}$ 11). This suggests that the crystallite size gradually increases as function of Mn doping. The calculated crystallite size of undoped CuO has been found as 19.54 nm, while 21.04, 24.03 and

21.00 nm for 1, 3 and 5% respectively. The increase in the crystallinity may be attributed to the difference in the ionic radii between Cu^{+2} (0.46 Å) and Mn^{+2} (0.73 Å). Same results also been indicated by T. Jiang et al. [80].

4.2 Morphological Investigations

Scanning electron microscope (SEM) has been used to observe the surface morphology of the prepared CuO samples. Figure 4.2 show the micrograph of Mn (1%, 3%, and 5%) doped CuO nanostructures.

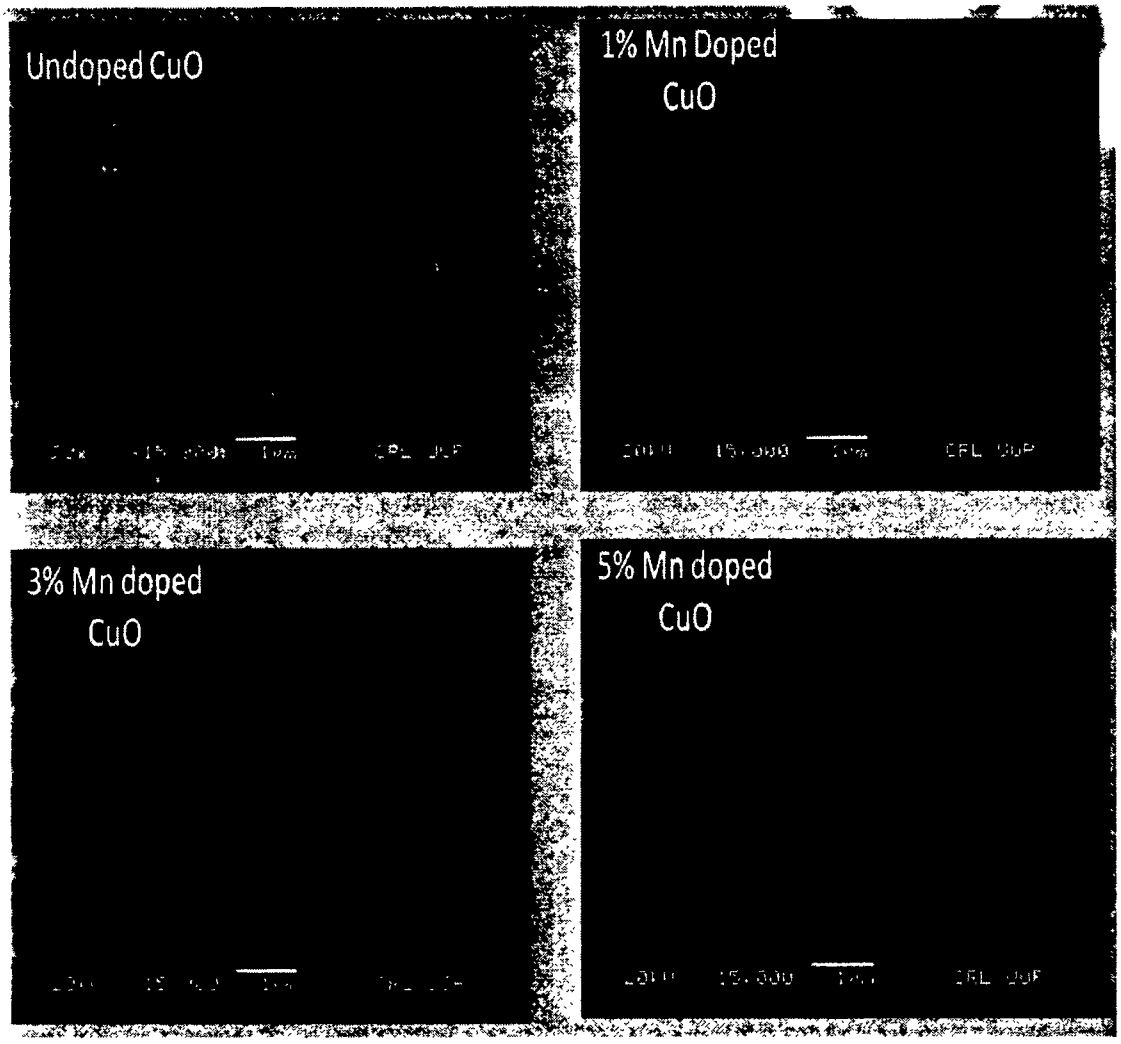

Fig. 4.2: SEM images of all prepared samples

The morphology of undoped CuO sample is found to be 1D nanostructure like as shown in the figure 4.2. It has been observed that the morphology changes from 1D Nanostructured like structure to 0D by increasing concentration of Mn doping. The same variation was also been observed in XRD patterns. The change in the morphology may also be attributed to the addition of surfactant which suppress the growth of nanostructures into rod like morphology and resist them into spherical shaped nanoparticles as also observed previously in Cr doped CuO [83].

4.3 Elemental Compositional Analysis

Energy dispersive x-ray spectroscopy (EDX) is used for elemental and compositional analysis which show the elemental analysis of pure and Mn doped CuO nanostructures.

Table 4.2- 4.6 listed the percentage content of the host (Cu and O) as well as doped (Mn) elements. Furthermore figure 4.3 (a, b, c and d) indicates the peaks of all elements present in the prepared CuO nanostructures. The EDX spectra show that no extra impurities have been present except Mn and host materials. The chlorine "Cl" peaks indicates that the samples were not washed well. However it has low concentration and percentage in the prepared samples.

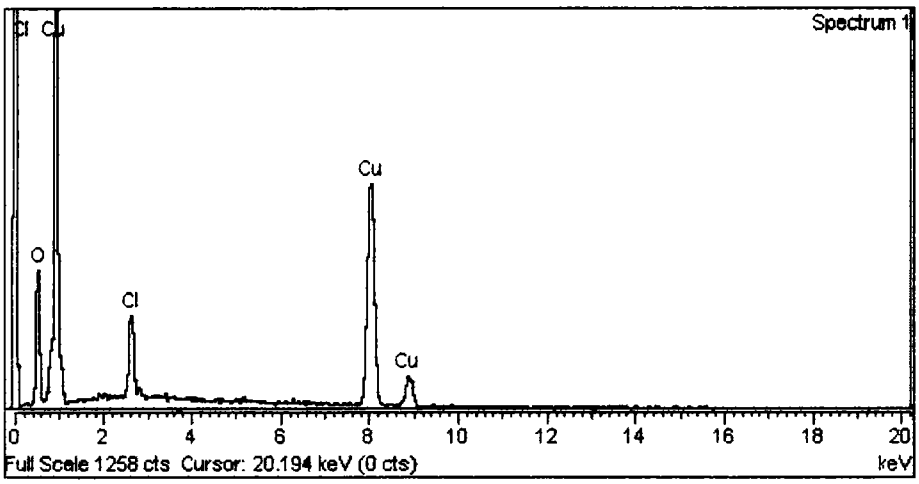

Fig. 4.3 (a): EDX spectrum of undoped CuO nanostructures

Table 4.2: Elemental compositions of the undoped CuO sample obtained from EDX spectrum

Element	Weight%	Atomic%
O K	18.56	46.22
Cl K	5.41	6.08
Cu K	76.04	47.69
Totals	100.00	100.00

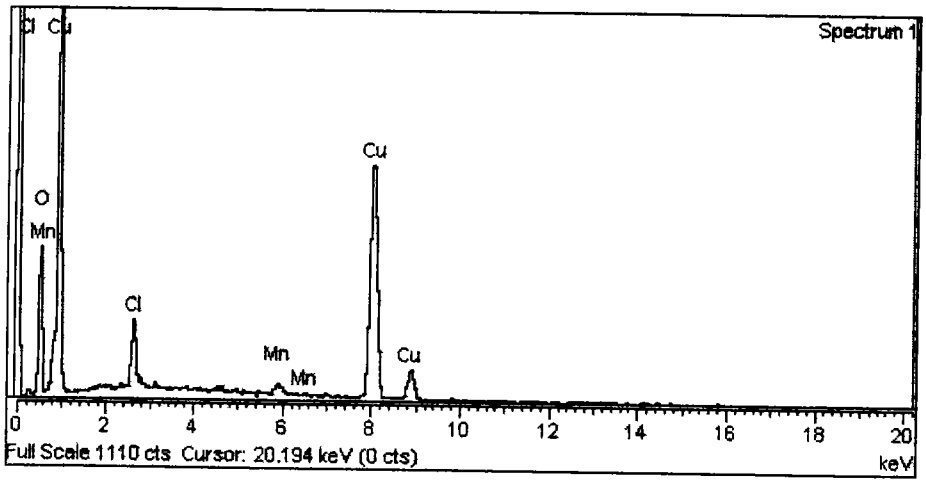

Fig. 4.3 (b): EDX spectrum of 1% Mn doped CuO nanostructures

Table 4.3: Elemental composition of 1% Mn doped CuO sample obtained from EDX spectrum

Element	Weight %	Atomic %
O K	19.07	47.31
Cl K	4.06	4.55
Mn K	1.24	0.89
Cu K	75.63	47.25
Totals	100.00	100.00

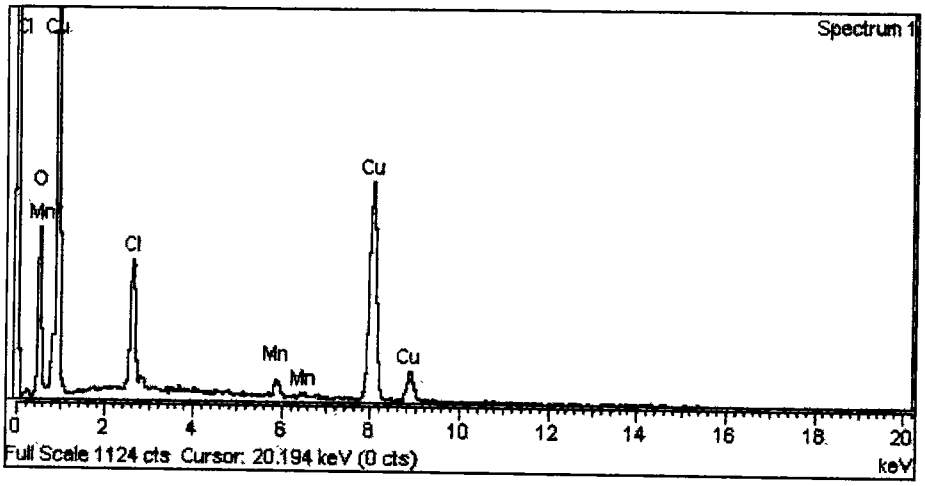

Fig. 4.3 (c): EDX spectrum of 3% doped CuO nanostructures

Table 4.4: Elemental composition of 3% Mn doped CuO sample obtained from EDX spectrum

Element	Weight%	Atomic%
O K	21.86	50.60
Cl K	7.89	8.25
Mn K	2.09	1.41
Cu K	68.17	39.74
Totals	100.00	100.00

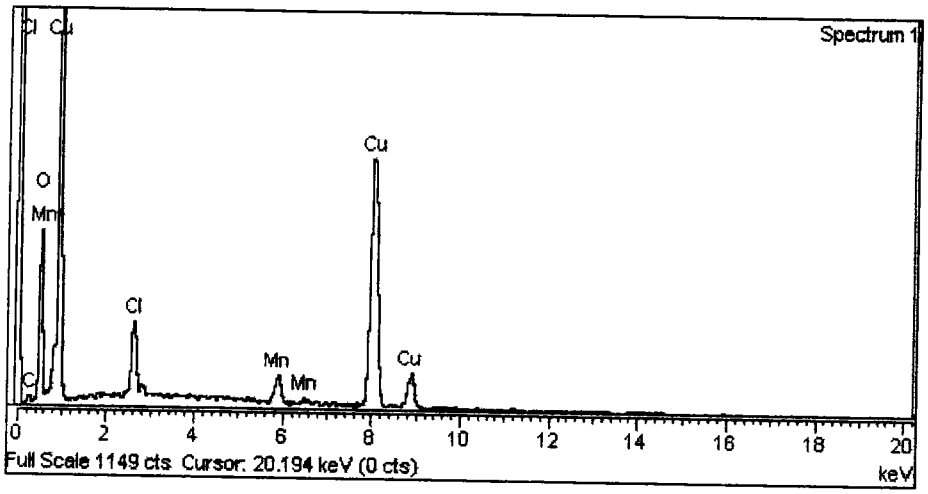

Fig. 4.3(d): EDX spectrum of 5% Mn doped CuO nanostructures

Table 4.5: Elemental composition of 5% Mn doped CuO sample obtained from EDX spectrum

Element	Weight%	Atomic%
C K	3.69	11.03
O K	19.41	43.50
Cl K	4.08	4.13
Mn K	3.04	1.98
Cu K	69.77	39.37
Totals	100.00	100.00

EDX spectra conform the presence of all elements in the synthesized samples according to their stichiometric ratio as specified at the time of experiment. The precursors used in the synthesis process results an extra peak of chlorine confirmed by all EDX spectra.

4.4 Study of Vibrational Moods

FTIR spectra of prepare undoped and Mn doped CuO nanostructures has been recorded in the wave number range from $400cm^{-1}$ to $4000cm^{-1}$ at room temperature as shown in figure 4.4. The Cu-O vibrations of monoclinic CuO are attributed to vibrational modes at 412, 491 and 611 cm^{-1}. Stretching mode of Cu-O has been observed at 441 cm^{-1} which assigned to B_{2g} mode of monoclinic structure of CuO [84]. The other evidence for the successful doping of Mn ions into CuO medium is the absence of the absorption modes related to secondary phases of MnO_2, CuO_2 and other possible impurities. Different vibrational modes of water molecule have been indicated by infrared absorption peaks in the range of 3000 – 3600 cm^{-1} which may be adsorbed at the surface of nanostructures during characterization [85].

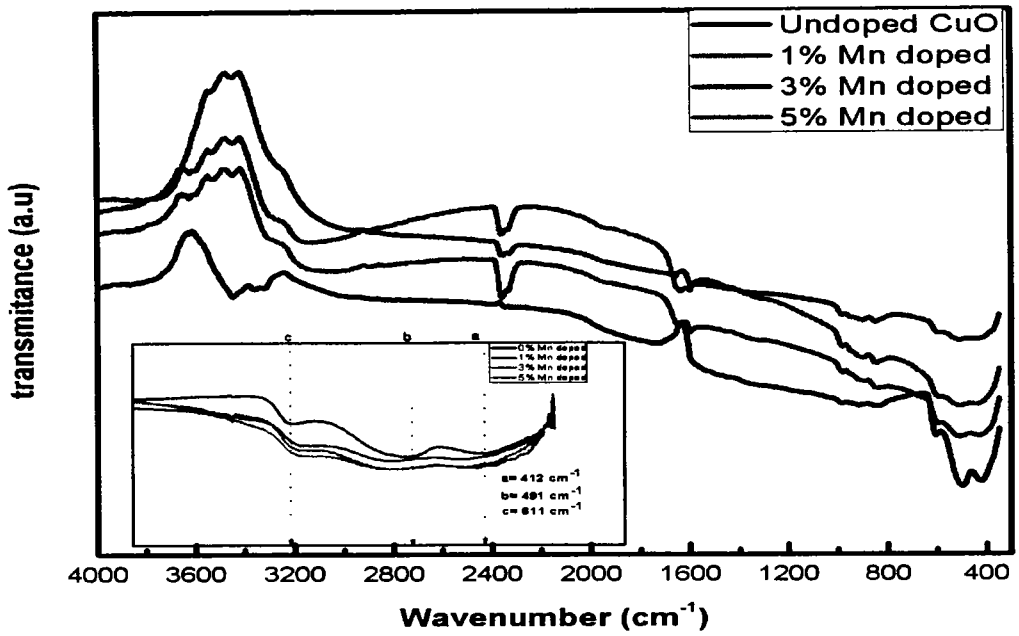

Fig. 4.4: FTIR spectra of undoped and Mn doped CuO nanostructures

4.5 Optical Properties

UV- Vis spectroscopy has been used to examine the optical properties of prepared undoped and Mn doped CuO nanostructures i.e. the effect of Mn on optical absorbance and band gap energies. Figure 4.5 shows the absorption spectra of undoped and Mn doped CuO nanostructures in the wavelength range of 200 – 800 nm at room temperature. The absorption peaks of all the samples have shows blue shift as a function of Mn doping into CuO. Tauc relation has been used to calculate the optical band gap energies of all the synthesized nanostructures [82].

$$\alpha h\upsilon = (h\upsilon - Eg)^n \qquad 4.1$$

Where α is the absorption coefficient, $h\nu$ is the photon energy, E_g is the optical band gap energy and "n" is an integer that takes value of 2 for a direct band gap and 1/2 for an indirect band gap.

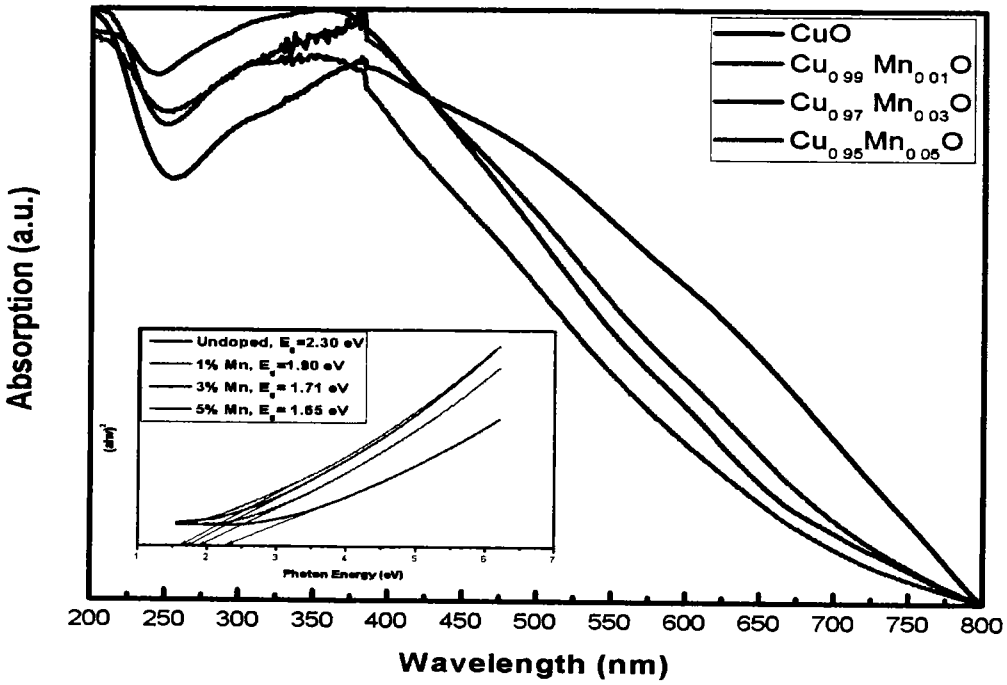

Fig. 4.5: UV-visible absorption spectra of the prepared nanostructures (Inset of the figure shows the band gap energy calculation)

The above graph shows the variation of $(\alpha h\nu)^2$ versus photon energy ($h\nu$) as function of using different Mn doping concentrations. In order to find the values of band gap energies, draw an extrapolating straight line in the above graph. By this it has been observed that the band gap energy of undoped CuO nanostructure is 2.30 eV which is higher as compare to bulk CuO (1.2 eV). This increase in the band gap of nanostructures is due to well known phenomenon of quantum confinement at nano scale. The values of band gaps on the photon energy axis has been found to be 1.90, 1.71 and 1.65 eV for 1%, 3% and 5% Mn doped CuO nanostructures respectively. The significant decrease in the band gap of Mn doped CuO may be due to the creation of band tail under the conduction band [86].

3.10 Dielectric Properties

All the measurements have been carried out at room temperature in the frequency range from 1 GHz to 3 GHz. The pallets of all the samples have been made by hydraulic press. Various parameters such as real and imaginary parts of dielectric constant have been calculated using standard formulas [87].

3.10.1 Real Part of Dielectric Constant

Figure 4.6 depicts the plot of real part of dielectric constant versus natural log of frequency. There is an increasing trend in dielectric constant by increasing the concentration of Mn as a dopant at low frequencies. It can be seen that the dielectric constant of undoped CuO is very low which has been increased significantly in case of 1% Mn doped CuO nanostructures. However, the value of dielectric constant has been decreased for all the samples at higher frequencies. This indicates that the doping of Mn in CuO has an impact on the dielectric relaxation properties of this system which can be explained on the basis of the Maxwell–Wagner interfacial type of polarization.

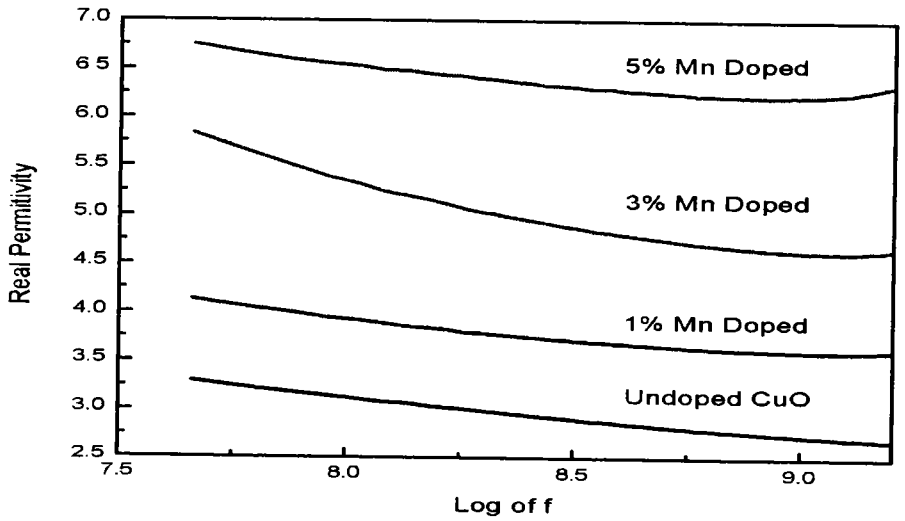

Fig. 4.6: Frequency dependent real part of dielectric constant

3.10.2 Imaginary Part of Dielectric Constant

The imaginary parts of dielectric constant versus natural log of frequency of prepared samples have been depicted in fig. 4.7. The imaginary part of dielectric constant has the same trend as that of its real part. The values of imaginary part of dielectric constant have an increasing trend at low frequencies by increasing the content Mn concentration. The dissipation factor (imaginary part of dielectric constant) also decreased at higher frequencies.

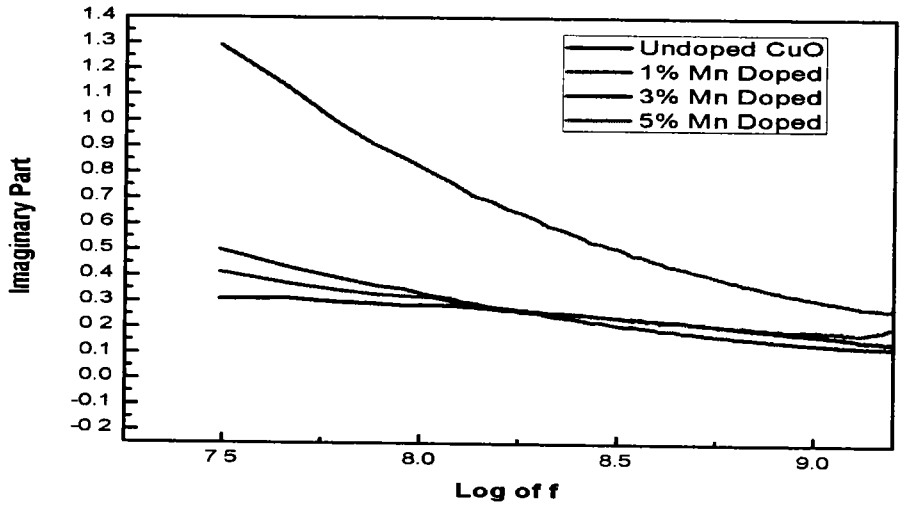

Fig. 4.7: Frequency dependent imaginary part of dielectric constant

3.11 Conclusion

Undoped and Mn doped CuO have been successfully synthesized via simple coprecipitation method. The prepared samples have been characterized using XRD, SEM, FTIR, UV-Vis spectroscopy and LCR meter.

The XRD patterns of synthesized undoped and Mn doped CuO nanostructures has confirmed the formation of monoclinic single phase having no extra peak of other impurities. XRD result also indicates the higher angle shift in the most intense peak i.e. $(\bar{1}11)$ which confirms the successful incorporation of Mn into CuO. SEM analysis suggests that undoped CuO has one dimensional like morphology which changes to zero dimensional as a concentration of Mn increases. From FTIR spectra, doped and undoped samples showed strong characteristic peaks of CuO in the range of 400 to 600 cm^{-1} which reveals that Mn has been successfully incorporated into the host matrix. EDS spectra have confirm the presence of copper, Mn and oxygen as major elements in the prepared samples. The energy band gap has been significantly tailored by Mn doping. This modification in the band edge can be attributed to the existence of donor impurity levels within the conduction band of CuO at nano level. The increase in the dielectric constant gives CuO much potential for its various applications i.e. solar cells. These prepared nanostructures with successful doping and tailored band gap are potential for future optical devices and nano medicines.

References

[1] H. Gleiter, *Acta Mater*: Vol. 48, pp.1, 2000.

[2] V. Skorokhod, A. Ragulya, I. Uvarova. *Academperiodica*: Vol. 30, pp. 180, 2001.

[3] S. Iijima, *Nature*: Vol. 354: pp. 56–58, 1991.

[4] A. E. Rakhshani, *Solid State Electron*: Vol. 29, pp. 7–17, 1986.

[5] Q. Zhang, K. Zhang, D. Xu, G. Yang, *Progress in Materials Science*: Vol. 60, pp. 208–337, 2014.

[6] J. Lorenzo, V. Moreno, A. A. Bustria, H. Kasai, *Cryst. Eng. Comm*: Vol. 16, pp. 2260-2065, 2014.

[7] O. Madelung. Semiconductors: data handbook. Berlin; New York: Springer; 2004.

[8] L. I. Berger, Semiconductor materials. Boca Raton, Fla. [u. a.]: CRC Press; 1997.

[9] J. Ghijsen, L. H. Tjeng, J. Vanelp, H. Eskes, J. Westerink, G. A. Sawatzky, *Phys Rev B*: Vol. 38, pp. 11322–30, 1988.

[10] D. P. Singh, O. N. Srivastava, J. Nanosci, *Nanotechnology*: Vol. 9, pp. 5345–50, 2009.

[11] A. S. Lane, R. S. Ningthoujam, S. J. Sharma, R. K. Vatsa, R. B. Pode, *Int. Jour. Of Nanotech*: Vol.7, pp. 979, 2010.

[12] M. K. Song, S. Park, F. M. Alamgir, J. Cho, M. Liu, *Material Science Eng R Rep*: Vol. 72: pp. 203–52. 2011.

[13] B. Meyer, A. Polity, D. Reppin, M. Becker, P. Hering, P. Klar, *Physics Status Solid (b)*: Vol. 249, pp. 1487–509 2012.

[14] S. Asbrink, L. J. Norrby, *Acta Crystallogr Sect A: Found Crystallogr*: Vol. 26, pp. 8–15, 1970.

[15] W. Y. Ching, Y. N. Xu, K. W. Wong, *Physical Review B* Vol: 40, pp. 7684–7695, 1989.

[16] Y. Cudennec, A. Lecerf, *European Journal of Solid State and Inorganic Chemistry*: Vol. 5, pp. 1471–1474, 2003.

[17] K. Santra, C. K. Sarkar, M. K. Mukherjee, B. Ghosh, *Thin Solid Films*: Vol. 213, pp. 226 – 229, 1992.

[18] H. H. Lin, C. Y. Wang, H. C. Shih, J. M. Chen, C. T. Hsieh, *Journal of Applied Physics*: Vol. 95, pp. 5889 – 5895, 2004.

[19] L. B. Luo, X. H. Wang, C. Xie, Z. J. Li , R. Lu , X. B. Yang. J. Lu, Luo, *Nanoscale Research Letters*: Vol. 9, pp. 637, 2014.

[20] C. Azzoni, A. Paleari, G. Parravicini, *J Physics Condence Matter*: Vol. 4, pp. 1359–66, 1992.

[21] A. Punnoose, H. Magnone, M. S. Seehra, J. Bonevich, *Physical Review B Condensed Matter and Materials Physics*: Vol. 64, pp. 174 420, 2001.

[22] S. Ravi, F. Winfred Shashikanth, *Materials Letters*: Vol. 141, pp. 132–134, 2015.

[23] X. M. Lin, A. C. S. Samia, J. Magn. *Magn. Mater*: Vol. 305, pp. 100, 2006.

[24] Z. Y. W, T. Yu, F. C. Cheong, X. J. Xu, C. T. Lim, V. B. C. Tan, *Nanotechnology*: Vol. 16, pp 88–92, 2005.

[25] Y. Li, J. Zhou, S. Tung, E. Schneider, S. Xi, *Powder Technol*: Vol. 196, pp. 89–101, 2009.

[26] H. T. Zhu, C. Y. Zhang, Y. M. Tang, J. X. Wang, *J Phys Chem C*: Vol.111, pp. 1646–50, 2007.

[27] S. Lee, S. U. S Choi, S. Li, J. A. Eastman, *J Heat Transfer*: Vol. 121: pp. 280–9. 1999.

[28] M. Vaseem, A. Umar, S. H. Kim, Y. B. Hahn, *J Phys Chem C*: Vol. 112, pp. 5729–35, 2008.

[29] K. Han M. Tao, *Solar Energy Materials and Solar Cells*: Vol. 93, pp. 153–157, 2009.

[30] A. Y. Oral, E. Mens, M. H. Aslan, E. Basaran, *Materials Chemistry and Physics*: Vol. 83, pp. 140–144, 2004.

[31] A. Aslani, V. Oroojpour, *Physica B: Condensed matter*: Vol. 406, pp. 144–149, 2011.

[32] M. L. Zhong, D. C. Zeng, Z. W. Liu, H. Y. Yu, X. C. Zhong, W. Q. Qiu, *Acta Materialia*: Vol. 58, pp. 5926–5932, 2010.

[33] H. Zhang, M. Zhang, *Materials Chemistry and Physics*: Vol. 108, pp. 184–187, 2010.

[34] Li, Xifei, C. Wang, *Journal of Materials Chemistry A*: Vol. 1.2, pp. 165-182, 2013.

[35] Z. S. Hong, Y. Cao, J. F. Deng, *Materials Letters*: Vol 52. pp. 34–38, 2002.

[36] S. Al-Amri, M. Shahnawaze Ansari, S. Rafique, M. Aldhahri, S. Rahimuddin, A. Azam, A. Memic. *Current Nanoscience*: Vol. 11, pp. 03, 2015.

[37] M. P. Neupane, Y. K. Kim, I. S. Park, K. Kim, M. H. Lee, T. S. Bae. *Surf Interface Analysis*: Vol. 41, pp. 259–63, 2009.

[38] T. Jan, J. Iqbal, U. Farooq, A. Gul, R. Abbasi, I. Ahmad, M. Malik; *Ceramics International*: Vol 41, pp. 13074–13079, 2015.

[39] A. S. Ethiraj, D. J. Kang, *Nanoscale Research Letters*: Vol 7, pp. 70, 2012.

[40] M. Azhar, M. K. Bhatnagar, *International Journal of Science and Research*: Vol 13, pp. 4–438, 2013.

[41] R. Al–Gaashania, S. Radimana, N. Tabetc, A. Razak Daud, *Journal of Alloys and Compounds*: Vol. 509 pp. 8761– 8769, 2011.

[42] H. Zhang, J. Feng, M. Zhang, *Materials Research*: Vol. 43, pp. 3221–3226 2008.

[43] T. Jan, J. Iqbal, Q. Mansoor, M. Ismail, M. S. H. Naqvi, A. Gul, S. F. H. Naqvi, F. Abbas, *J. Phys. D: Appl. Phys*: Vol 47, pp. 7, 2014.

[44] M. shahmiri, N. Azowa, Norhazlin, Zainuddin, N. Asim, Bakhtyar, Zaharim, Sopian, *WSEAS Transaction on environment and development*: Vol. 9, pp. 02, 2013.

[45] B. Toboonsung, P. Singjai, *Journal of Alloys and Compounds*: Vol. 509, pp. 4132–4137, 2011.

[46] Y. I. Erdogan, O. Gullu, *Journal of Alloys and Compounds*: Vol. 492, pp. 378–383, 2010.

[47] Z. Yunling, L. Yan, Z .Nan, L Xiulin, Bull, *Material. Science*: Vol. 34, pp. 967–971, 2011.

[48] S. Harish, M. Navaneethan, J. Archana, S. Ponnusamy, C. Muthamizhchelvan, Y. Hayakawa, *Material Letters*: Vol. 10, 2015.

[49] A. Tischner, A. Käck, T. Maier, C. Edtmaier, C. Gspan, G. Kothleitner: *Microelectronic Eng 86 1258,* 2009.

[50] S. Franssila: *Introduction to microfabrication,* John Wiley and sons, 2004.

[51] M. DiVentra, S. Evoy, J. R. Heflin: *Introduction to Nanoscale science and Technology*, Kluwer Academic Publishers, 2004.

[52] C. Koch, J. D. Whittenberge, Intermetallics Vol. 4, pp. 339, 1996.

[53] R. Janot, D. Guerard, Progress in Materials Science: Vol. 50, pp. 1 2005.

[54] Thakur Prasad Yadav, Ram Manohar Yadav, Dinesh Pratap Singh, *Nanoscience and Nanotechnology*, Vol 2(3): pp. 22–48, 2012.

[55] A. Tischner, A. Kack, T. Maier, C. Edtmaier, C. Gspan, G. Kothleitner, *Microelectronic Engineering*: Vol. 86.4, pp. 1258-1261, 2009.

[56] L. Qin, J. Xu, X. Dong, Q. Pan, Z. Cheng, Q. Xiang, *Nanotechnology*: Vol.19 pp. 185705, 2008.

[57] Y. Liu, E. Koep, Meilin; *Chem. Mater.* Vol *17,* pp. 3997–4000 2005.

[58] Handbook of Nanophase and Nanostructured Materials pp 102-144

[59] Q. Zhang, K. Zhang, D. Xu, G. Yang, H. Huang, F. Nie, C. Liu, S. Yang, *Progress in Materials Science* Vol 208–337, pp 60, 2014.

[60] Y. Xia, P. Yang, Y. Sun, Y. Wu, B. Mayers, B. Gates, *Advance Material*: Vol. 15, pp. 353–89. 2003.

[61] J. Park, J. Joo, S.G. Kwon, Y. Jang, T. Hyeon, *Chem Int Ed*: Vol. 46. pp. 4630–60, 2007.

[62] R. Devan, R. Patil, J. Lin, Y. Ma, *Adv Funct Mater*: Vol 22:33 pp. 26–70. 2012.

[63] K. Byrappa, T. Adschiri *Progress in Crystal Growth and Characterization of Materials* Vol 53 pp. 117–166 2007.

[64] R. Roy, *J. Solid State Chem*: Vol. 111, pp. 1–17, 1994.

[65] J. C. Robert, Y.L. Cars, *J. Sol–Gel Sci. Technol*: Vol. 2.1-3, pp. 707-710, 1994.

[66] D. M. Turley, *Materials Science and Engineering*: Vol. 19.1, pp. 79-86, 1975.

[67] G. S. Chung, *Journal of Physics*: Vol.3, pp. 63, 1960.

[68] A. G. Michette, S.A. Pfauntsch, the first hundred years, Chichester, New York: John Wiley and Sons, 262, 1966.

[69] Prosini, P. Paolo, D. Zane, M. Pasquali, *Electrochimica. Acta*: Vol. *46, pp. 3517,* 2001.

[70] J. Almer, S. R. Stock, *Journal of Structural Biology*: Vol. 157.2. pp. 365-370, 2007.

[71] S. L. Flegler, J. W. Heckman, K. L. Klomparens, Scanning and Transmission Electron Microscopy: an introduction, New York: Oxford University Press, 225, 1955.

[72] J. Pawley, *Scanning Electron Microscopy*: Vol. 19, pp. 324–336, 1997.

[73] Z. L. Wang, *J. Phys. Chem. B,* Vol 104, pp. 1153–1175, 2000.

[74] Z. L. Wang, *Weinheim ; Wiley–VCH, Characterization of nanophase materials, New York* 20001.

[75] P. Poizot, S. Laruelle, S. Grugeon, L. Dupont, J. M. Tarascon, *Nature*: Vol 407, pp: 496–499, 2000.

[76] Thermo Nicolet Corporation, Introduction to Fourier Transform Infrared Spectrometry, Thermo Nicolet Corporation Documentation, 2001.

[77] B. Faure, G. S. Alvarez, A. Ahniyaz, I. Villaluenga, G. Berriozabal, Y. R. D. Miguel, L. Bergstrom, *Sci. Technol. Adv. Mater*: Vol. 14, pp. 23, 2013.

[78] G. J. Exarhos, Butterworth–Heinemann Manning Boston Greenwich Characterization of optical materials. Materials characterization series, UK 1993.

[79] S. Perkowitz, D. G. Seller W. M. Duncan, *J. Res. Natl. Inst. Stand. Technol*: Vol. 99, pp. 605, 1994.

[80] T. Jiang, J. Kong, Y. Wang, D. Meng, D. Wangl, M. Yu, *Cryst. Res. Technol*: Vol. 51, pp. 58–64 2016.

[81] S. Mohebb, S. Molaei, A. R. J. Azar, *Journal of Applied Chemistry*: Vol. 8, pp. 27-30, 1997.

[82] Y. Gulen, F. Bayansal, B. S. ahin, H. A. C. etinkar, H. S. Guder, *Ceramics International*: Vol. 39 pp. 6475–6480, 2013.

[83] S. Mohebbi, S. Molaei, A. R. J. Azar, *Journal of Applied Chemistry*: Vol. 8, pp. 27-30, 1997.

[84] K. Karthik, N. M. Kanagaraj, S. Arumugam, *Solid State Commun*: Vol. 151, pp. 564–568, 1997.

[85] V. Vellora, T. Padil, M. Cernik, *Int. J. of Nanomed*: Vol. 8, pp. 889–898, 2013.

[86] Y. S. Yu, G.Y. Kim, B. H. Min, S. C. Kim, *Journal of the European Ceramic Society*: Vol. 24, pp. 1865–1868, 2004.

[87] H. Mahmoudi Chenari, A. Hassanzadeh, M. M. Golzan, H. Sedghi, M. Talebian, *Current AppliedPhysics*: Vol. 11, pp. 409-413, 2011.